BCR signaling and dynamic micropatterns

Elmeri Kiviluoto

Master´s thesis

University of Turku
Institute of Biomedicine
26.11.2021

Master´s degree in Biomedical Imaging
Light Microscopy Imaging

Credits: 20

Supervisors:

1: PhD. Pieta Mattila

2: Sara Hernández Pérez, MSc

Passed:

Grade:

UNIVERSITY OF TURKU
Faculty of Medicine
Institute of Biomedicine

ELMERI KIVILUOTO: BCR signaling and dynamic micropatterns.

Master's thesis, 50 pp., 1 Appendices
November 2021

Abstract

B lymphocytes (B cells) are an important part of the adaptive immune system. Recognition of surface presented antigen, typically on antigen presenting cell (APC), by the B cell receptor (BCR) triggers BCR signaling cascades leading to recruitment of the cytoskeleton and formation of a specialized cell-cell interaction structure, the immunological synapse (IS) on the interface of the APC and B cell. BCR activation ultimately leads to B cell differentiation into an antibody secreting plasma cell or a memory B cell.

Studying the dynamic process of B cell activation presents a challenge, requiring spatial and temporal control over antigen presentation. Micropatterning of functional molecules allows control over cell placement. From many different micropatterning technologies, UV-lithography provides a cost-effective method for creating quality functional micropatterns on a glass substrate.

In this work, I used poly-L-lysine-graft-polyethylene-glycol-biotin (PLL-g-PEG-biotin) coated glass coverslips with fibronectin patterning to control B cell attachment. In our dynamic micropatterns, temporal control of B cell activation is achieved via streptavidin-α IgM Fab acting as a surrogate antigen that binds the PLL-g-PEG-biotin outside the micropattern after cell attachment. Coverslips were imaged with spinning disk confocal or Airyscan confocal microscopy. Images of cells were segmented into separate regions of interest (ROI) and fluorescence intensities were measured inside these ROIs.

This study shows that 1) functional coating of micropatterns was repeatable and highly specific, 2) spatial and temporal control of B cell activation was successful and 3) that enrichment of BCR signaling molecules Btk and PLCγ2 in the cell adhesion plane correlate with areas of antigen engagement.

KEYWORDS: Micropatterning, B cells, B cell receptor, Image analysis, Spinning disk confocal microscopy, Live cell imaging, Super-resolution imaging

List of abbreviations:

antigen presenting cell (APC)

B cell adaptor protein (BCAP)

B cell linker (BLNK)

B cell receptor (BCR)

bimolecular fluorescence complementation assay (BiFC)

bivalent anti-BCR antibody fragment (F(ab')2)

blue native polyacrylamide gel electrophoresis (BN-PAGE)

Bruton's tyrosine kinase (Btk)

central supramolecular activation cluster (cSMAC)

class II major histocompatibility complex (MCHII)

common lymphoid progenitor cell (CLP)

complete RPMI (cRPMI)

deep ultraviolet (DUV)

diacylglycerol (DAG)

extracellular matrix (ECM)

extracellular signal-regulated kinase (ERK)

ezrin, radixin and moesin (ERM)

forkhead box protein O1 (FOXO)

Föster/fluorescence resonance energy transfer (FRET)

hematopoietic stem cell (HSC)

immunological synapse (IS)

inositol 1,4,5-trisphosphate (IP3)

interleukin-7 receptor (IL7R)

laser direct-write (LDW)

light-induced molecular adsorption (LIMAP)

membrane immunoglobulin (mIg)

mitogen-activated protein kinase (MAPK)

monovalent antibody fragment (Fab)

nuclear factor kappa-light-chain-enhancer of activated B cells (NF-κB)

phosphate buffered saline (PBS)

phosphatidylinositol (3,4,5)-trisphosphate (PIP3)

phosphatidylinositol 4,5-bisphosphate (PIP2)

phospholipase Cγ2 (PLCγ2)

poly-L-lysine-graft-polyethylene-glycol-biotin (PLL-g-PEG-biotin)

polydimethylsiloxane (PDMS)

proximity ligation assay (PLA)

region of interest (ROI)

scientific complementary metal–oxide–semiconductor (sCMOS)
supramolecular activation cluster (SMAC)
tag image file format (TIFF)
tyrosine-based activation motif (ITAM)
Wiskott-Aldrich syndrome protein (WASP)

Table of Contents

1 REVIEW OF THE LITERATURE

1.1 Adaptive Immune-System

The immune system protects the body from invading pathogens such as foreign microbes and parasites and keeps the body's own tissues in check by screening and terminating cells that have been infected by viruses or turned malignant and potentially cancerous. The immune system has two separate but interacting branches working in parallel, called innate and adaptive immunity. Innate immunity has evolved earlier and has effective yet unspecific response to pathogens. Part of it acts as physical barrier, the epithelia, against entry by the pathogen. If this barrier fails, cells of the innate immunity can recognize common molecular patterns found in pathogens, but they always mount the same type and strength of response regardless of the type of pathogen. Among these responses are production of cytokines, activation of complement, and removal of foreign substances by phagocytosis. Quick response to a pathogen by the innate immunity contrasts with the adaptive immunity which takes longer to develop after encounter with the pathogen. Though these two branches of the immune system are distinct, they help each other by signaling and stimulating each other's function e.g., via cytokines. (Abbas et al., 2021)

The adaptive branch of the immune system has two main features: specificity and memory. Unlike innate immunity, adaptive immunity builds a specific response against a pathogen. The adaptive immune system recognizes antigens, molecular structures of the pathogen and creates antibodies that bind specifically to the antigen to neutralize and/or mark it for destruction by other parts of the immune system, such as phagocytes. It also recognizes the body's own cells that are infected, damaged, or have turned malignant and either instructs them to go under apoptosis or kills them. Recognition of an antigen by the adaptive immune system leads to the formation of immunological memory specifically against the recognized antigen so that subsequent infections by pathogen carrying the same antigen epitopes are swiftly stifled.

B and T lymphocytes are the immune cells that carry out the functions of the adaptive immune system in vertebrates. Upon pathogen infiltration, lymphocytes along with other immune cells coordinate the immune response via cytokines and antibodies. Lymphocytes originate, like all blood cells, from hematopoietic stem cells (HSCs) in the bone marrow. From HSCs, develop common progenitors of all lymphocytes and lymphatic line dendritic cells, the common lymphoid progenitor cells (CLPs). The differentiation from CLPs to immature lymphocytes cells takes place in the bone marrow, after which B cells continue their maturation in the bone marrow and immature T cells translocate to thymus.

1.2 B cells

B cells are a group of lymphocytes that specialize in the humoral immune response of the adaptive immune system and formation of immunological memory. Process of B cell maturation, or development, from CLPs to mature B cells happens in the bone marrow after birth and in fetal-liver before birth (Abbas et al., 2021).

First step of B cell development is proliferation. This creates a large pool of progenitor cells that undergoes rearrangement of the immunoglobulin receptor genes coding for the heavy and light chains of the B cell receptor in a process called V(D)J recombination. This creates a wide repertoire of unique antigen recognizing receptors to account for the variability of antigens occurring in nature. Genes of the immunoglobulin molecules of the BCR are arranged in the genome as segments; constant (C), variable (V), and joining (J). (Abbas et al., 2021)

In V(D)J recombination pro B cells, derived from CLPs, first rearrange their D and J segments to create a μ heavy chain which is further joined with the upstream V region, advancing them to pre-B cell stage (Pieper et al., 2013). The pre-B cells express a pre-B-cell antigen receptor which is a paring of the μ heavy chain with a surrogate light chain called V-preB and lambda-like. Signaled by the pre-B-cell antigen receptor, the μ heavy chain is joined with a rearranged kappa and lambda chains of the V region (Pieper et al., 2013). By combining different combinations of V, D and J segments a pool of cells each having a different combination is created. The resulting BCRs' epitope binding sites have different affinities for any one antigen epitope, result of which is a vast repertoire of immature B cells, all expressing IgM type BCRs with a different variable region on their surface. The immature B cells migrate to the spleen for further differentiation as part of the maturation progress. (Abbas et al., 2021)

1.2.1 BCR signaling

The B cell surface receptor, B cell receptor (BCR), is a transmembrane receptor consisting of the IgM or IgD type membrane immunoglobulin (mIg), and two additional transmembrane proteins, Igα and Igβ organized as a heterodimer. The BCR binds its cognate antigen with its mIg variable regions complementary to the epitope of the antigen. This causes the BCR to trigger intracellular signaling pathways that lead to immunological activation of the B cell. BCR signaling is a dynamic, highly regulated process both spatially and temporally. BCR works together with its co-receptor CD19 and other membrane molecules to activate multiple signaling cascades inside the cell (Kuokkanen et al., 2015). In addition, BCR exhibits tonic signaling, a low-level constitutive signaling that happens irrespective of antigen binding on the BCR (Kuokkanen et al., 2015). BCR signaling comprises of large, complex network of multiple intracellular pathways which lead to activation of transcription factors and subsequently

expression of genes associated with B cell activation, cell survival and proliferation (Harwood and Batista, 2010).

In vivo, B cells encounter antigen presented on the surface of antigen presenting cells (APC). The formation of an antigen/BCR complex activates cytosolic signaling cascade, the first step of which is phosphorylation of immunoreceptor tyrosine-based activation motifs (ITAM) on cytosolic tails of Igα/Igβ heterodimer by Src family tyrosine-protein kinase Lyn. Phosphorylation of ITAMs of Igα/Igβ leads to recruitment of tyrosine-protein kinase Syk to the BCR. (Wen et al., 2019)

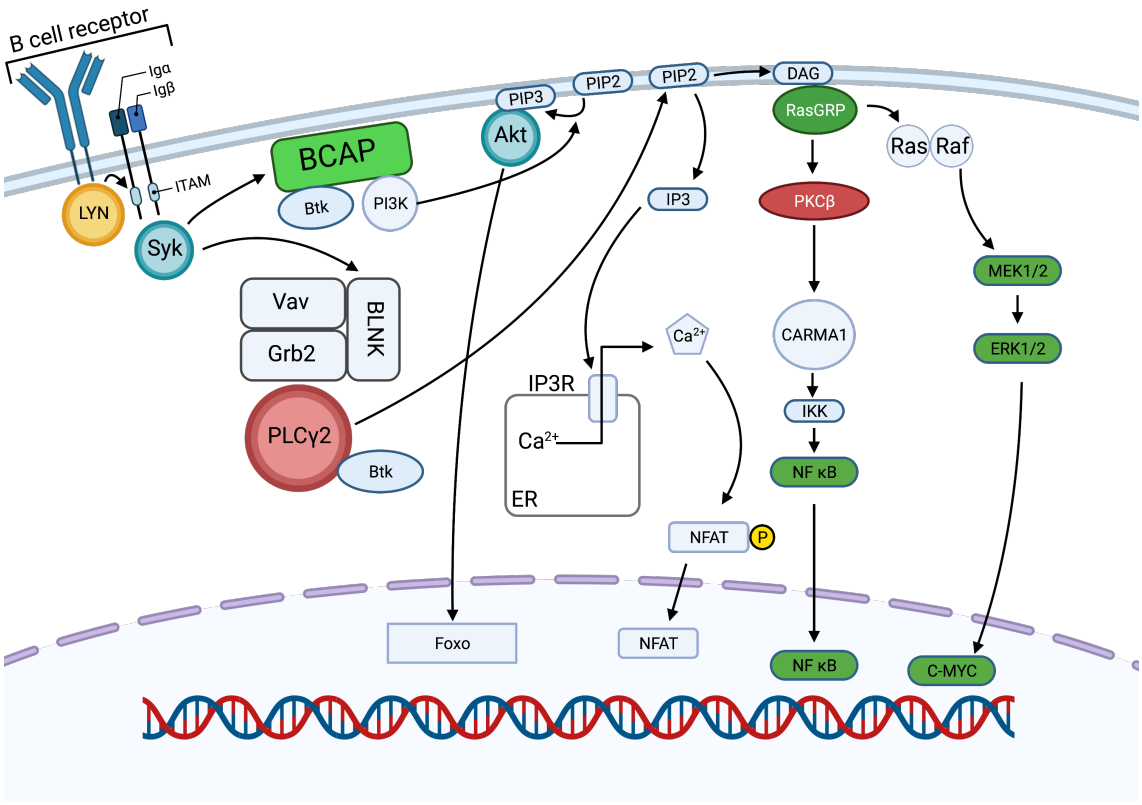

Figure 1. BCR signaling network. BCR activation upon antigen binding triggers phosphorylation of ITAM sequences of Igα/Igβ by Lyn. ITAMs then recruit Syk, which can then phosphorylate adapter proteins BCAP and BLNK for gathering and activation of several signaling pathways which lead to regulation of antigen internalization and activation of transcription factors and gene expression in the nucleus, regulating maturation and differentiation of the B cell.

BCR/Syk takes part in the phosphorylation key adaptor proteins B cell linker (BLNK) and B cell adaptor protein (BCAP) which then form complexes with proteins taking part in multiple signaling pathways. (Wen et al., 2019)

Bruton's tyrosine kinase (Btk) and phospholipase Cγ2 (PLCγ2) are phosphorylated upon recruitment by BLNK which leads them to produce diacylglycerol (DAG) and inositol 1,4,5-trisphosphate (IP3) from phosphatidylinositol 4,5-bisphosphate (PIP2) in the cell membrane. Production of DAG triggers a pathway leading to activation of nuclear factor kappa-light-chain-enhancer of activated B cells (NF-κB) and its translocation into the nucleus. (Wen et al., 2019; Kurosaki, 2002)

IP3 binds and opens IP3 receptor which functions as a Ca^{2+} channel in the endoplasmic reticulum, leading to release of Ca^{2+} to the cytosol. Further downstream, this leads to dephosphorylation nuclear factor of activated T-cells in and its translocation to the nucleus. (Müller and Rao, 2010)

PI3K is recruited to BCAP via the help of CD19 and is then phosphorylated. Phosphorylated PI3K activates Btk and Akt via generation phosphatidylinositol (3,4,5)-trisphosphate (PIP3) from PIP2. This is followed by activation of Akt and its translocation to the nucleus, where it inactivates transcription factor Forkhead box protein O1. (Okkenhaug and Burger, 2015)

DAG binds and activates RAS guanyl-releasing protein which triggers the mitogen-activated protein kinase / extracellular signal-regulated kinase (MAPK/ERK) pathway leading to translocation of ERK into the nucleus and activation of c-Myc transcription factor. (Wen et al., 2019; Yasuda, 2015)

The nuclear factors entering the B cell nucleus change the transcription of genes affecting various cellular processes. NF-κB promotes transcription of genes taking part in development and function of lymphocytes and nuclear factor of activated T-cells has been found essential in development of B-1a cells (Berland and Wortis, 2003; Rawlings et al., 2006). Downregulation of FOXO changes the transcription of interleukin-7 receptor (IL7R) and Rag genes among others, affecting B cell development and differentiation (Amin and Schlissel, 2008). Likewise, MAPK/ERK pathway has been found to be important in B cell development by regulating immunoglobulin gene rearrangement and pre-B cell proliferation (Yasuda, 2015).

In addition, the signaling cascades initiated by the BCR is the internalization of antigen complexed with BCR for processing and presentation (Avalos and Ploegh, 2014). Ultimately, the signaling by the BCR leads to the maturation and differentiation of the B cell to an antigen secreting plasma cell or a memory B cell (Harwood and Batista, 2010).

Internalization of BCR/antigen complex happens in endocytosis, after which the antigen particles are processed into peptides and loaded into class II major histocompatibility complexes (MCHIIs). In this context, the B cell functions as a professional antigen-presenting cell (APC) for CD4 positive helper T cells. The T cell receptor recognizes the MHCII/antigen complex and activates the B cell leading to further B cell differentiation. In addition to recognizing free antigens from blood and lymph, B cells detect antigen on the surface of other APCs such as dendritic cells. (Adler et al., 2017)

1.2.2 BCR activation models

The mechanism by which the formation of BCR/antigen complex is relayed to intracellular ITAM phosphorylation and consequent start of the intracellular signaling is a topic of debate and inquiry in the field. Also, little is known about the membrane organization of BCR in nonactivated cells. Multiple competing yet possibly

complementary models of BCR activation have been proposed. The issue, as of yet, has not been solved with structural studies of BCR/antigen complex since no meaningful conformational change between the unbound and bound state of the BCR with antigen has been discovered. (Harwood and Batista, 2010)

Experiments on BCR activation have focused on using anti-BCR antibodies that bind to the invariable region of the mIg, thus functioning as a surrogate for physiological antigen. It has been shown that bivalent anti-BCR antibody fragments (F(ab')2) induce BCR signaling when binding to the BCR and that monovalent anti-BCR antibody fragments (Fab) do this only when attached to a surface but not in soluble form (Woodruff et al., 1967; Tolar et al., 2009a). Currently, several models exist for the mechanism of BCR activation.

Conformational change model focuses on the conformational change in the immunoglobulin molecule of BCR after antigen binding. Shen and colleagues (2019) observed conformational changes in the heavy chain of membrane-bound Ig and between it and Igβ by site-specific labelling and Föster/fluorescence resonance energy transfer (FRET). It is notable that no evidence of conformational change propagating to the membrane proximal part of mIg has been found in structural studies of the mIg (Davies et al., 1990; Davies and Metzger, 1983; Metzger, 1978).

The receptor cross-linking, or conformation-induced oligomerization model, proposes that BCRs are monomeric at a resting state of the cell and cross-link upon binding with multivalent antigen, leading to BCR activation and signaling (Feng et al., 2020; Harwood and Batista, 2010). Conformation-induced oligomerization model is supported by FRET studies on cytoplasmically tagged BCR, Igα, and Igβ (Tolar et al., 2005). However, the high FRET signal even before the stimulation and its sensitivity for molecular orientation and proportions of tagged molecules makes interpretations on the evidence cautious (Kuokkanen et al., 2015). A study using TIRF microscopy on multiple BCR mutants supports receptor clustering upon BCR activation by discovering that a membrane-proximal domain of the mIg, Cμ4, becomes exposed when antigen is bound by the BCR, which is then followed by clustering of the BCRs (Tolar et al., 2009b). This suggests that BCRs are not directly cross-linked to each other by means of evenly spaced antigen epitopes but rather induced to oligomerize after binding to antigen, whether monovalent or multivalent.

The conformation-induced oligomerization model states that free BCRs get immobilized upon antigen binding and then form clusters with their Fc regions. The primary factor that favors conformation-induced oligomerization model to conformational change model is that it accounts for the fact that surface-bound monovalent antigens, such as lipid bilayer bound antigens, do lead to BCR activation and thus excludes the necessity of direct BCR cross-linking (Avalos and Ploegh, 2014; Li et al., 2019; Tolar et al., 2009b).

Dissociation activation model started on the observation that after cell lysis the BCRs appeared in oligomeric state in blue native polyacrylamide gel electrophoresis (BN-PAGE) (Schamel and Reth, 2000). In dissociation activation model, BCRs auto-inhibit their activation in the resting state by existing as oligomers. Upon binding with its cognate antigen, BCRs are separated, and Igα/Igβ ITAMs are exposed for phosphorylation (Feng et al., 2020; Harwood and Batista, 2010). This model has been supported by bimolecular fluorescence complementation assays (BiFC), and proximity ligation assays (PLA) among synthetic biology approaches where coexpressed mutant BCR and tyrosine kinases Syk and Lyn were studied in Drosophila (Yang and Reth, 2010; Kläsener et al., 2014). PLA assays allowed measurement of endogenous BCRs with the downside of following only small amounts of interactions at a time, which means that deriving a conclusion on the organization of hundreds of thousands of receptors is difficult.

1.3 Actin cytoskeleton

The cell cytoskeleton is a network of different filaments providing mechanical support, expandability and contractility providing movement for the cell, vesicle transport, and structural platform on which different components of cellular signaling cascades organize as well as means to transmit extra- and intracellular signals (Bezanilla et al., 2015).

Networks of cytoskeletal filaments of F-actin form the actin cytoskeleton. The different structures created by the actin cytoskeleton are highly dynamic and at constant flux; Polymers are continually degraded to and assembled from monomers, filaments are bundled and capped. (Bezanilla et al., 2015)

There are few distinct dynamic actin structures in the cell. Membrane protrusions in a finger-like shape, perpendicular to the leading edge of the cell, are filopodia, formed by long actin fibers under the cell surface. Lamellipodia are sheet-like protrusions of branched actin and are a key structure in cell locomotion. Cortical actin network, or actin cortex, is a mesh-like structure of actin filaments that are connected to cell membrane via linker proteins such as ezrin, radixin and moesin (ERM) proteins, septins, filamins and protein 4.1 in a juxtaposed manner. (Mattila et al., 2016)

Recently, the lymphocyte cytoskeleton is emerging as a regulatory apparatus for signaling through the cell membrane and specifically immune receptor activation. This is demonstrated in the many pathologies caused by the dysfunction of the actin cytoskeleton. For example, Wiskott-Aldrich syndrome protein (WASP) is a specific activator of Arp2/3, a key regulator of actin polymerization, and is defected in immune dysfunction causing Wiskott-Aldrich syndrome. Other important regulators of actin cytoskeleton, such as Rho family GTPases Cdc42 and Rac, are also important in the activation and development of B cells (Walmsley et al., 2003; Heasman and Ridley, 2008; Burbage et al., 2015; Arana et al., 2008; Brezski and Monroe, 2007). Actin cytoskeleton affects the distribution of BCR in the cell surface by restricting its movement on the membrane,

where BCRs exist in nanoclusters, heterogenous in size and composition (Mattila et al., 2016).

1.4 Immunological synapse

Upon encountering an antigen presented on the surface of an APC, and consequent activation of the BCR and intracellular signaling pathways, an immunological synapse (IS) forms at the site of antigen recognition. The IS forms between the APC and B cell in a two-stage manner (Fleire et al., 2006). The actin cytoskeleton is recruited to spread the cell membrane over the APC, allowing for the gathering of more antigen by the B cell. The antigen, bound to BCR, is concentrated onto signaling hot-spots, microclusters, via reorganization of actin cytoskeleton. Myosin, associated with the actin cytoskeleton then contracts the cell membrane, leading to the maturation of the IS. The B cell/APC IS is a cell-cell structure where BCR-antigen complexes, with other membrane proteins, form concentric structures called supramolecular activation clusters (SMAC). The main structure, comprising of BCR/antigen rich central SMAC (cSMAC) and surrounding peripheral SMAC (pSMAC), rich in actin and adhesion molecules, is similar to synapses of other lymphocytes. However, the B cell IS is a site of not only signaling but also for internalization of the gathered BCR/antigen complexes for further processing of the antigen. (Mattila et al., 2016; Kuokkanen et al., 2015)

While B cells can activate through recognition of soluble antigen, antigen presented in the surface of an APC can be more concentrated and internalized with higher efficiency, as discover in vitro studies (Batista and Neuberger, 2000).

1.5 Micropatterns

Micropatterning aims to reconstitute one or more aspects of the physiological *in situ* microenvironment of cells *in vitro* or apply specific environmental stimuli in a controlled and highly reproducible manner. These can be the physical, such as the geometry and architecture, or chemical composition, such as patterning of ligands for surface receptors, of the microenvironment. A multitude of micropatterning techniques are available for cell and molecular scientists. These techniques vary in accuracy, speed, dimensionality, substrate options, and cost, and their applications are also varied (Carpi et al., 2011).

Many micropatterning techniques modify the existing cell culturing method of seeding cells onto glass substrates such as coverslips by adding patterned microscopic features on them.

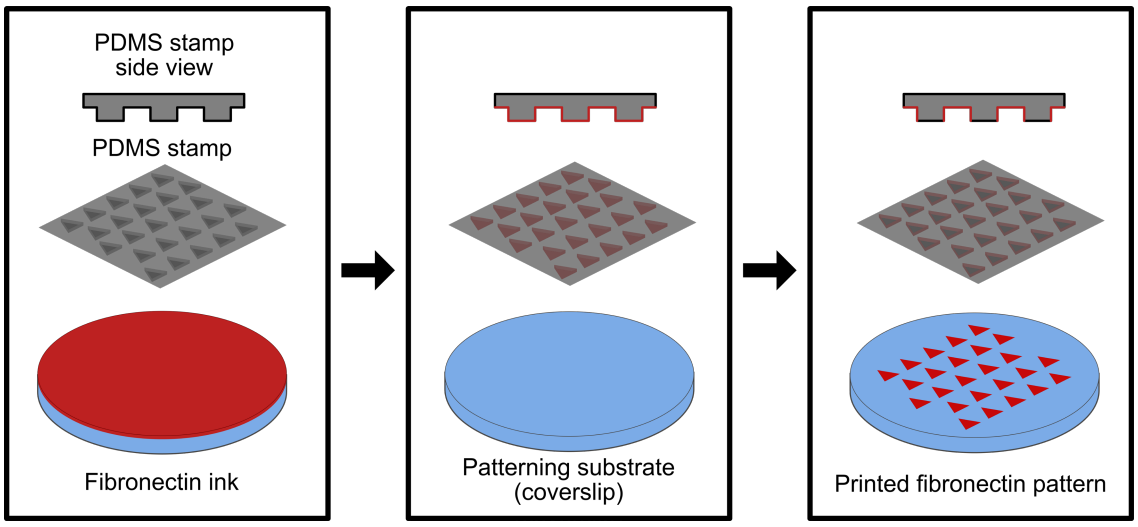

Figure 2. Microcontact printing method for production of micropatterned substances on a glass substrate. A PDMS stamp with raised surface features in a pattern is pressed into ink, a protein that adheres to the PDMS such as fibronectin, transferring it to the stamp. The stamp is then pressed on the surface of choosing, on which the stamp leaves a film of the ink protein in the form of the pattern. Illustration not to scale.

One of the most common micropatterning technique is microcontact printing (figure 2), where a polydimethylsiloxane (PDMS) stamp, with the desired microscopic features in it, is coated with a protein of choice and is then pressed on the glass substrate to create a micropattern of the protein on the coverslip (Théry, 2010). Microcontact printing has been used to create microscopic patterns of extracellular matrix (ECM) proteins on top of glass substrates to induce integrin-mediated adhesion of the cell to the pattern. This method has been used to study cell adhesion, the development of focal adhesions, and actin stress fibers (Théry, 2010)

3D micropatterning allows a more comprehensive mimicry of the cell microenvironment. 3D matrices can support the cells from all dimensions and allow self-organization. Inverted microcontact printing has been used to create functionalized microwells in polystyrene (Dusseiller et al., 2005). Softer substrates, such as polyacrylamide, can be micropatterned with microfabricated stencils or microcontact printing. Multiple techniques such as electric potential, light, or pH can be used to change the physicochemical properties of the micropatterned substrates, allowing dynamic control of the microenvironment.

In inkjet cell printing, cells are deposited on a substrate in droplets from a printer device. A commercial thermal inkjet printer can be modified to print biological material, such as *E.coli,* onto rigid substrates with a 0.1mm dot size and density of 400 dots per square centimeter (Zheng et al., 2011). Drop-on-demand inkjet printing method allows for precise control of cell deposition and multilayered 3D printing of cells onto substrates such as glass microscope slides and microtiter plates. This method has been used to create multilayer 3D structures of different cell types for drug evaluation (Matsusaki et al., 2013). Electrohydrodynamic jet printing has been used to print ECM proteins, such

as fibronectin and extracellular matrix glycoprotein, and 3-aminopropyltriethoxysilane and is capable of producing dot sizes from 200 to 0.5 μm using a pyroelectrohydrodynamic jet.

Optical and electric methods of cell patterning allow researchers to use the physical properties of cells, instead of their surface adhesion to molecules of the ECM, to pattern cells. Electrophoretic patterning of cells takes advantage of the negative surface charge of live mammalian cells to array them in a direct current electric field (Ozkan et al., 2003). This method allows aseptic handling and monitoring of cells through transparent electrodes that sandwich the cell medium. Optical tweezers use radiation pressure and electric fields to trap and move dielectric objects, such as single cells, with a laser beam. The downside of this method is the limited area and resolution as well as challenges with the size of objects able to be moved (Kim et al., 2017; Ozkan et al., 2003). Energy levels of the laser output can also cause photodamage. Optoelectronic tweezers can overcome these challenges by using non-coherent light to create dielectrophoresis electrodes on a photoconductive surface allowing electrophoretic manipulation of microparticles or cells (Chiou et al., 2005). Optoelectronic tweezers use 100 000 less optical intensity than optical tweezers and allow parallel manipulation of thousands of particles over a hundred-fold larger area than optical tweezers.

Cells can be patterned by transferring them from a source film to an acceptor substrate via laser-based direct writing. Most of the laser-based direct writing techniques fall under the moniker laser direct-write (LDW). LDW techniques use a ribbon that is transparent to laser light and has been coated with the cells of interest on one side. A laser pulse through the ribbon volatilizes it in a designed manner, propelling the cell from the ribbon onto a substrate coated with a bio-polymer or culture medium. LDW techniques allow the user to design their own patterns and support various materials and cell types with high precision. Laser-guided direct writing is a technique analogous with optical tweezers that uses a continuous laser and optical fibers to move cells from a liquid suspension to a receiving substrate over a small distance <1cm. (Schiele et al., 2010)

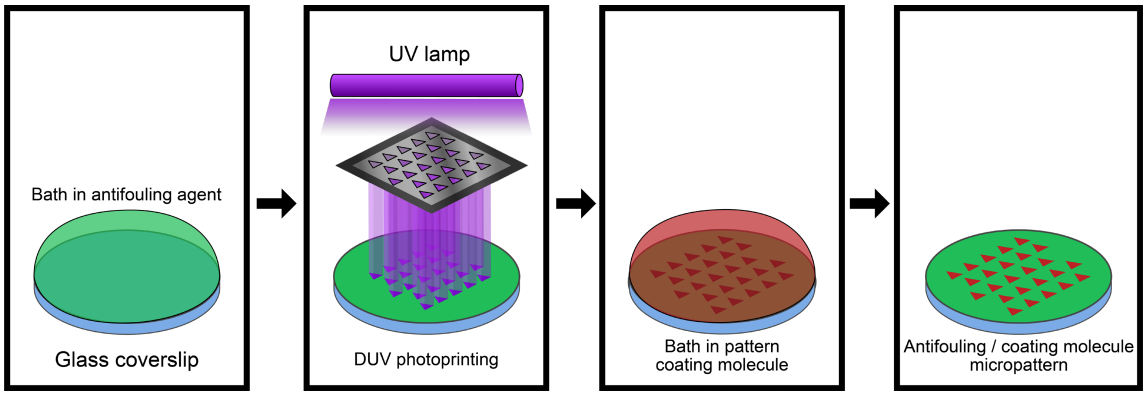

Figure 3. Deep ultra-violet (DUV) micropatterning method for production of glass coverslips with micropatterned substance surrounded with antifouling agent. A coverslip coated with antifouling agent is

irradiated with DUV light trough a photomask. The irradiated part can then be coated with glass adhering molecules, creating a patterned coverslip. Illustration not to scale.

In deep ultraviolet (DUV) micropatterning, DUV light is used to irradiate a passivated substrate, such as glass or PDMS, through a photomask to create micropatterns (figure 3). The photomask is made from quartz and has a chromium layer with micropatterns etched on it. When the photomask is illuminated with DUV light from the chrome side, an image of the micropatterns projected on the substrate attached on the other side of the mask through the transparent pattern.To passivate the substrate, such as a glass coverslip, before photoprinting, it is coated with an antifouling agent, commonly PLL-g-PEG. The antifouling agent is destroyed in the UV light, leaving an antifouling free area in the shape of the pattern in the photomask. This micropatterning method has been used to create cell adhesive micropatterns with fibronectin. (Carpi et al., 2011)
A newer and less common UV micropatterning method is Light-Induced Molecular Adsorption (LIMAP), where the use of photomask is omitted for the pattern is created with the spatial light modulator in an epifluorescence light microscope. In this technique, the pattern is etched with a UV light onto a glass coverslip. Similarly, the coverslip is coated with an antifouling agent, which is destroyed in the etching. The use of spatial light modulators such as digital micromirror devices allows changing the pattern shape and size without additional cost, unlike in the photomask method, where a new mask is needed for a new pattern. The LIMAP technique also allows for easy multiplexed micropatterning as multiple patterns can easily be aligned by fluorescence of the previous pattern.(Strale et al., 2016). Additionally, the use of anchoring molecules in LIMAP has made it possible to pattern virtually any protein on a glass surface and thus allowed attachment of poorly adhering cells and proteins to glass coverslips while also improving their patterning selectivity and homogeneity (Watson et al., 2021)

Table 1. Micropatterning methods and their advantages and disadvantages. Modified from (Martinez-Rivas et al., 2017)

Technique	Patterned substance	Advantage	Disadvantage
Inkjet printing	Individual small cells, bacteria	Moderate cost Good controllability	Droplet formation Requires an external power source
Optical and optoelectronic cell trapping	From single to thousands of cells or micro particles	Remote and large-scale manipulation	Thermal effects and photodamage in cells

		Highly specific due to the intrinsic charge and dielectric properties of cells	Requires an external power source
Laser-based cell patterning	Individual cells and particles	Cells and any particles can be manipulated	Large instrumentation Complex set-up
Acoustic patterning	Individual cells limited by the area of the patterning surface	No significant heat generation and no effects on cell viability	Requires an external power source, piezoelectric surface, and electrode fabrication.
Dielectrophoresis	Groups of cells	Combine electrokinetic forces with hydrodynamic effects High-resolution patterning Large-scale parallel manipulation	Requires an external power source Dielectric force decreases due to the separation distance of electrodes
Magnetic techniques	Individual cells labelled with magnetic particles	Remote manipulation High-resolution patterning, No stress behavior on cells	Magnets and labelling cells with magnetic particles are required
Surface chemistry methodologies	Molecules aiding the cell patterning such as cell adhesion proteins	High precision and recognition by receptor or specific functional groups between the surface and cells	Pretreated surface is required The surface chemistry could modify the functionality of cells
Microcontact printing	Dyes made of the desired molecule stamped on a substrate such as glass	Low cost, rapid prototyping	Difficulty in controlling the ink and the surface robustness
Microwells and filtration	PDMS stamp or a porous substrate holes evaporated to create a micropattern	Minimize the surface chemistry and conservation of cell functionality	Time consuming placing numerous cells inside microwells

Deep UV (DUV) micropatterning	Molecules on the surface of a substrate such as glass are deactivated by patterned light	Does not require expensive facilities	The resolution depends on the photomask design and patterning substrate

In this project, we have optimized a novel application of DUV micropatterning to control and monitor B cell activation *in vitro*. This was achieved by using fibronectin pattern to direct cell adhesion and PLL-g-PEG-biotin as a linker protein to attach anti-BCR antibody fragments to a glass surface. The selective attachment of anti-BCR antibody fragments allows us to control the area and timing of the B cell activation. This coupled with the imaging compatibility of the glass substrate on which the micropatterns are created allows us to monitor B cell activation from the very beginning. Our dynamic micropatterns can help in elucidating the complexity of both BCR signaling and its regulation through dynamic organization of the actin cytoskeleton in the initial stages of B cell activation.

2. AIMS

Aims of this project are:

- To optimize the preparation and use of dynamic micropatterns in B cell activation
- To show that dynamic micropatterns successfully allow control over the spatial and temporal initiation of B cell activation
- To monitor the activity of BCR signaling and cell spreading during B cell activation

3. MATERIALS AND METHODS

3.1 Cell culture

A20 lymphoma mouse B lymphocytes stably expressing hen egg lysozyme-specific IgM BCR (D1.3) (Williams et al., 1994) were cultured in complete RPMI (cRPMI) made with RPMI-1640 medium with 2.05 mM L-glutamine supplemented to 4 mM L-Glutamine, 10 mM HEPES, 10% fetal calf serum, 50 µM Beta-mercaptoethanol and 100 U/ml penicillin/streptomycin.

3.2 Cell transfection

Cell transfection for live imaging was done as described in (Šuštar et al., 2018):

2 million A20 D1.3 cell were transfected with 2 µg of plasmid encoding LifeAct Emerald, kindly gifted by Guillaume Jacquemet, in 2S transfection buffer (5mM KCl, 15 mM $MgCl_2$, 15 mM HEPES, 50 mM Sodium Succinate, 180mM Na_2HPO_4/NaH_2PO_4 pH 7.2). Electroporation was carried out in 0.2 cm gap width electroporation cuvettes (Sigma-Aldrich) with AMAXA Nucleofector II (Lonza) using program X-005. After transfection, the cells were cultured O/N in cRPMI complemented to FCS 20% and DMSO 1% and used in a live-imaging experiment.

3.3 Coverslip preparation and micropattern printing

3.3.1 Cleaning the coverslips

13 mm Ø glass coverslips were rinsed in succession with denatured ethanol in concentration of 70% and 94% in a 24-well plate after which the coverslips were transferred onto a piece of tissue paper under a plastic or cardboard cover for the ethanol to evaporate. The coverslips were then moved to a glass plate and UV-cleaned in a Stratagene UV Stratalinker 2400 for 15 min.

3.3.2 Coating of coverslips and micropattern printing

UV-cleaned coverslips (13 mm Ø) were coated with 2 µg of PLL (poly-L-lysine)-graft-PEG (poly ethylene glycol)-biotin (PLL(20)-g[3.5]- PEG(2)/PEG(3.4)- biotin(50%), SuSoS) in a wet chamber for 1h at room temperature and subsequently rinsed 2-3 times with phosphate buffered saline (PBS, Sigma-Aldrich) on a 24 well plate. To print the patterns a quartz glass mask (Delta Mask) with the following specifications was used: 5 x 5 x 0.09 inches with anti-reflective chrome coating on one side, with smallest structure size of 1.5 +/- 0.5 µm and maximum defect density of 0.1 defects/cm^2, and approximated curve of 0.1 µm. The mask was cleaned in succession with MilliQ water, 70 % EtOH and 94% EtOH, dried with pressured air and UV-cleaned in Jelight Company UVO Cleaner 342-220 for 5 minutes. The photomask contains 8 segments of different patterns of which

a segment with patterned circular 5 µm diameter dots 20 µm apart from each other in x and y directions was used for micropatterning. PLL-g-PEG-biotin coated coverslips were attached to the quartz photomask on the side opposite to the chrome coating, onto an area with the chosen pattern. This was done by first pipetting a 4 µl-droplet of water, one per coverslip, on the photomask and then transferring the coverslips over the water droplets such that the PLL-g-PEG-biotin coated side faced the surface of the photomask. Excess water was then removed gently with a paper tissue. To secure the coverslips in place, a clear plastic film was applied over the coverslips and adhered to the photomask by pipetting water between the plastic film and the photomask interface in the periphery of the mask. UV printing of the patterns happened in the Jelight Company UVO Cleaner. The photomask with the coverslips attached was placed in the UVO cleaner, chrome side of the mask facing the light source, for 6 minutes so that the light source shined through the chrome coated back side of the photomask and created an image of the micropattern onto the coverslip, destroying the PLL-g-PEG-biotin coating in the shape of the pattern. After removing the plastic film by hand, the coverslips, now with micropatterns imprinted, where detached from the photomask by pipetting MilliQ water onto the photomask. After the water had dissociated the coverslips from the photomask surface, they were removed with metal tweezers and left to dry on a piece of tissue paper, coated side facing up, shielded from dust with a cardboard or plastic covering. After drying at room temperature, the coverslips could be coated (3.2.3) right away or stored in +4 °C, shielded from light for up to one month.

3.3.3 Pattern coating with fibrinogen/fibronectin

The coverslips imprinted with micropatterns were coated with 10 µg/ml of fibronectin from bovine plasma (Sigma-Aldrich) and 10 µg/ml of human fibrinogen AlexaFluor 546 conjugate (Thermo Fisher Scientific) for 1h in room temperature wet chamber shielded from light. The coverslips were then rinsed with PBS 2-3 times on a 24-well plate (24-wp). Enough PBS was left in the well after final rinsing step to cover the coverslips, ensuring that they would not dry out. Quality of the patterns was then visually inspected with EVOS M5000 epifluorescence microscope (AMF5000, Thermo Fisher Scientific) and coverslips with the best overall quality were selected for experiments, and coverslips with bad pattern quality (uneven coating, blurred patterns or elliptical shape) were discarded.

3.4 Activation of B cells on the micropatterns

3.4.1. Seeding of cell onto micropatterns

For fixed samples: Coverslips were transferred onto a new 24-wp with 300 µl/coverslip of cRPMI and approximately 200 000 A20 D1.3 cells in 200 µl/well of cRPMI was pipetted on top. The 24-wp was then incubated in the incubator (37°C, 5% CO_2) for at least 10

minutes. After 10 minutes the coverslips were inspected visually with a transmitted light microscope and, if density of cells attached to patterns was considered sufficient, experiment was continued. If not, the samples were incubated for an additional 10 minutes and evaluated again after that time. Coverslips on the 24-wp were washed with 5-10 ml of cRPMI 1 to 3 times to remove the unbound cells.

For live imaging: The printed coverslips were attached onto the bottom of a 35 mm confocal dish (MatTek) with melted Parafilm to create an imaging chamber. 100-150 µl of cRPMI with 200 000 A20 D1.3 cells was pipetted on to the coverslip surface of the chamber and cells were then allowed to attach to micropatterns for ~10 minutes at 37°C, 5% CO_2. The coverslip surface was then washed two to three times with fresh culturing medium while keeping the coverslip surface always immersed.

3.4.2 Immunological activation

To activate the B cells, we used a streptavidin-α IgM Fab conjugate. Streptavidin binds to the biotin with high affinity and anchors the Fab fragment onto the coverslip, outside the patterned cells. The α IgM Fab bound on the coverslip surface binds to the BCR, triggering B cell activation.

For fixed samples: 0.5 µg/600 µl/coverslip of strep-α IgM Fab (Goat Anti-Mouse IgM, Fab, µ Specific (115-007-020), Jackson ImmunoResearch Laboratories, conjugated to streptavidin using Streptavidin Conjugation Kit - Lightning-Link® (ab102921), Abcam) conjugate was added on top of the medium in the 24-wp where it attached to PLL-g-PEG-biotin. The coverslips were then transferred to 37°C 5% CO_2. Kinetics of B cell activation on micropatterns were tested by modifying the time between adding of streptavidin Fab and fixation. For activated cells, two fixing times were used: after 5 min and 15 min of adding the streptavidin Fab. 0-minute time point cells were not activated, but fixed right after washing. As a negative control, 0.5 µg/600 µl/coverslip of α IgM Fab (Jackson ImmunoResearch Laboratories, (115-007-020)) without streptavidin was used to assess that cell activation does not happen without Fab attachment on the coverslip.

For live imaging: The MatTek chambers with cells attached as described in 3.3.1 were transferred inside the microscope's environment chamber, set at 37°C. Images were acquired using a spinning disk confocal microscope as described in 3.5.3. Images were acquired for 30-60s (no-activation condition) followed by activation with 0.5 µg/coverslip of strep-α IgM Fab diluted in total volume of 20 µl of cRPMI, and continue recording every 1-10 seconds for an additional 12-17 minutes with inter-experimental variation on the frequency and length of acquisition.

3.4.3 Immunofluorescence

For quality inspection of micropatterning, coverslips with PLL-g-PEG-biotin and fibronectin micropatterning were created as described and then incubated in culture medium with α IgM antibody Fab fragments with and without streptavidin conjugation and then washed 2-3x with PBS and stained with Donkey anti-Goat IgG (H+L) Cross-Adsorbed Secondary Antibody (Thermo Fisher Scientific) labelled with AlexaFluor 488 for 1h at room temperature inside a wet chamber.

For fixed samples, the coverslips were fixed after 5 or 15 min of activation by adding 16% PFA solution to a final concentration of 4% PFA and incubated for 10 minutes at RT. Samples were blocked with Donkey blocking buffer consisting of 5% Donkey Serum (Jackson Immunoresearch) and 0.1% Triton X-100 in PBS for 20 min at room temperature and stained with immunofluorescence antibodies for phosphorylated Btk (pBtk) and phosphorylated pPLCγ2 (pPLCγ2), and phalloidin (Table 2) for 1 hour in room temperature or overnight in +4°C while shielded from light. Samples were washed three times with PBS and coverslips were mounted on a 25 mm x 75 mm x 1.0 mm glass microscope slide with 4 µl/coverslip of Fluoromount-G, with DAPI (Thermo Fisher Scientific).

Table 2. Antibodies and labels used in immunofluorescence

REAGENT	**CATALOG NO. / MANUFACTURER**	**DILUTION (IN PBS)**
Acti-stain 670 phalloidin	PHDN1 / Cytoskeleton	1:200
Alexa Fluor 488 Mouse Anti-Btk (pY223)/Itk (pY180)	564847 / BD Biosciences	1:100
Alexa Fluor 488 Mouse Anti-PLCg2 (py759)	558507 / BD Biosciences	1:100
Donkey anti-Goat IgG (H+L) Cross-Adsorbed Secondary Antibody, Alexa Fluor 488	A-11055 / Thermo Fisher Scientific	1:500

3.5 Imaging

3.5.1 Fixed sample imaging with 3i CSU-W1 Spinning disk confocal microscope

Fixed samples were imaged with 3i CSU-W1 Spinning disk confocal microscope equipped with Photometrics Prime BSI sCMOS camera and using a Plan-Apochromat 63x/1.4 Oil DIC M27 objective. Filters and lasers are described in Table 3.

Table 3. Laser specifications and filters used in confocal spinning disk imaging

SOLID STATE LASER WAVELENGTH (nm)	POWER (mW)	FILTERS		
405	100	DAPI (445/45nm)		
488	150	GFP (525/30nm)		Quad Band (550/40 nm, 521/21 nm, 607/34 nm, 700/45 nm)
561	150	Cy3/Alexa (617/73nm)	568	
640	100	Cy5/Alexa (692/40nm)	647	

A single optical section of cell-pattern interface was captured. Cells were selected by eye for imaging based on if they were sitting on the fibronectin/fibrinogen pattern and looked intact. Some images contained multiple separate cells.

3.5.2 Fixed sample imaging with Airyscan confocal scanning microscope

The Zeiss LSM 880 with Airyscan was used for super-resolution imaging of fixed samples. A Zeiss C Plan-Apochromat 63x/1.4 Oil DIC M27 objective was used with 633nm HeNe laser, BP 570-620 + LP 645 filters and 32-channel Airyscan Hexagonal element detector. Images with size of 720 x 720 pixels and real size of 26.99 µm x 26.99 µm were acquired and processed using Zen 2.3 SP1 Black software. Images were processed using the auto settings, 2.49 AU pinhole and 4% laser power.

3.5.3 Live imaging

Live imaging of A20 D1.3 cells was carried out with 3i CSU-W1 Spinning disk confocal microscope equipped with a Hamamatsu sCMOS Orca Flash4.0 camera using Plan-Apochromat 63x/1.4 Oil DIC M27 objective. Filters and lasers are the same as described in Table 2 except for 561 nm laser which had maximum power of 100 mW.

3.6 Image processing and analysis

Images were acquired in SlideBook Slide file format (.sld) and they were imported into ImageJ FIJI (NHI) with BioFormats plug-in in Tag Image File Format (TIFF) format. One ImageJ macro script was written to save the imported images, a second on for semi-automatic cropping of the TIFF images and third macro for quantitative analysis of the ingested images.

3.6.2 Image analysis of confocal 2D images of fixed B cell activated on dynamic micropatterns

The 2D confocal images were analyzed with FIJI Version 1.51 23 April 2018. Bio-Formats and SlideBook plugins were used to read and convert SlideBook Slide files to individual TIFF files. This process was partly automated by a macro written in ImageJ macro language. This file conversion macro needed manual opening of images with the Bio-Formats plug-in. After a set of images had been opened on ImageJ, the macro could be run. The macro first requests the user to specify a directory for the saved images and then saves the images individually to the given directory.

All images containing multiple cells were cropped to create images containing only one cell and one fibronectin dot. The image cropping macro, created to do this semiautomatically, would ask the user for a directory with images in it. After specifying a directory, the macro asks for another directory to save the result images. The macro then enters a loop (For-loop 1) that repeats the subsequent steps for each image in the input directory, before exiting. In the For-loop 1, the macro opens an image from the image directory and prompts the user to give a number that corresponds to how many cells the user wants to crop to individual images from the opened image. The macro enters another loop (For-loop 2) that repeats this user-given number of times. In the beginning of the For-loop 2, the macro creates a selection rectangle on the image and asks the user to place it on top of any cell on the image and to confirm the selection. During this step the user can manipulate the selection. After confirmation by the user, the macro copies the image area in the selection and creates a new image from the copied area, which it then saves in the results folder with the name of the original image, concatenated with a number that is iterated by one every time the For-loop 2 iterates. After the specified number of cropped images has been created and saved, the macro exits the For-loop 2 and continues iteration of the For-loop 1 by opening a new image from the image folder which. After all images in the image folder have been worked on, For-loop 1 will complete, and the macro will close all open windows and terminate.

A third ImageJ macro was written to analyze the cropped images generated by the image cropping macro. The image measurement macro requires: a folder with images that contain only one cell and no other features in the user defined cell segmentation channel (specified later), and only one micropattern feature, such as a dot, per image. The macro starts by asking the user for a directory with images that the user wants analyzed, called input directory. The macro then asks for an output directory, which can be any folder other than the input directory, and this folder is used for saving the results of the image analysis macro. The macro also asks the user to type a filename, which is used as a template for naming the results files and is concatenated with an iterating number to make the results files' names unique. Lastly, the macro asks the user to specify the

numbers of the two channels that: have only the micropattern features visible, and are used to segment the cell from the background, in our case channel 3 (561 nm) and channel 4 (640 nm), respectively. The macro then starts the analysis of the images in the input folder by opening one image file in ImageJ and duplicating it. This duplicate's channels are then split into separate images. The channel image with micropattern features visible is then segmented by automatically setting a threshold value with using the Huang2 method, followed by the same for the channel selected by the user for cell segmentation, creating binary images of the two channels. Next, the binary cell image is applied with ”fill holes” command which changes any negative value pixels that are surrounded by group of positive value pixels into positive value pixels, effectively closing the positive value pixel group that represents the cell. The image is then applied with five iterations of morphological operation called dilate followed by five iterations of another morphological operation called erode. After this, the macro uses the binary cell image to create a mask of the cells. This is done by using the ”Analyze particles…” command in ImageJ, which detects groups of positive value pixels in the binary image. The macro sets the command to ignore particles with size of 20 μm2 or less to make sure only the cell will be analyzed. The ”Analyze particles…” command outputs a region of interest (ROI) which is the outline of the detected particle, the cell in this case. The macro does the same for the binary image of the pattern feature without applying morphological operations, yielding a second ROI of the pattern outline. A third ROI is created by subtracting the pattern ROI from the cell ROI. This cell-minus-pattern ROI outlines the cell area that is outside the pattern. The macro uses ImageJ's multi-measure command to measure and calculate properties of the three ROIs and image values inside the areas outlined by them from all channels of the original opened image. The macro outputs the values into a table, which the macro then saves as a csv file in the output directory. This is followed by closing all the windows in ImageJ. The macro continues by opening the next image file in the input directory and starting the analysis again. In order to not overwrite previous results, the results filename specified by the user is concatenated with a number, starting from zero, that is iterated by adding one to it every time a new image is opened from the input folder. After all images in the input folder have been opened once, the macro will stop opening images after last analysis step and will stop after closing all ImageJ windows for the last time.

The pattern ROI was subtracted from the cell ROI using this script inside the macro:

```
roiManager("select", 0);
setKeyDown("alt");
roiManager("select", 1);
setKeyDown("none");
```

```
roiManager("add");
roiManager("select", 2);
roiManager("rename", "Doughnut");
```

Image values inside all three ROIs were calculated from all image channels of the original cropped image with the multi-measure command. Measurements used were area, mean gray value, and roundness.

3.6.3 Image analysis of confocal images of fibronectin micropatterns

Spinning disk confocal 2D images containing only fibronectin patterns were converted to TIFF and saved as in 3.6.2. Image segmentation was done on uncropped images and happened as for the fibronectin dots in 3.6.2. ROI creation and measurement was done as in 3.6.2 with the exception of using only the fluorescent fibrinogen channel for measurements.

3.7 Statistics and data presentation

Statistical analysis of the acquired data was done with Graph Pad Prism software (version 8.0.3, GraphPad Software Inc.). Paired Student's t-test was applied to the data, unless stated otherwise, to compare significance of the difference between different test conditions. Significance, as p-values, is always denoted as: * < 0.05 p, ** < 0.01 p, *** < 0.001 p, **** < 0.0001 p. Super Plots (Lord et al., 2020) of the data where prepared, whenever possible, in Graph Pad Prism. Schematics were created in Affinity Designer, Adobe Illustrator and Adobe Photoshop.

4. RESULTS

Purpose of the project was to optimize the fabrication of dynamic DUV micropatterns for the study of B cell immunological activation and to observe the enrichment of phosphorylated PLCγ2 and Btk signaling proteins in the cell spreading phase of the activation. With fibronectin dot pattern surrounded by PLL-g-PEG-biotin, dynamic micropatterns enabled us to control the transition of B cells from a steady state to BCR stimulated state both in terms of the location of the activation and its timing. This was made possible by using monovalent antigen binding fragments (Fab) of α IgM antibodies ligated with streptavidin (strep-α IgM Fab), binding to the PLL-g-PEG-biotin, that target Fc region of the BCR causing robust activation only in surface presented form. This means that the B cells bound on the fibronectin features of the pattern are activated at the time when strep-α IgM Fab is added to the solution and only at the outside the fibronectin pattern, where the cells can sense the strep-α IgM Fab molecules bound by biotin. This was then followed by spreading of the cellular membrane over the strep-α

IgM Fab - PLL-g-PEG-biotin area surrounding the cell as the cell seeks the surrogate antigen.

The DUV micropatterning technique described by Carpi and colleagues (2011) was adapted to create a fibronectin dot micropattern on PLL-g-PEG-biotin coated Ø 13 mm coverslips. Ø 5 µm dots were selected because of their radially symmetric shape and right size so that a B cell can occupy the whole dot at steady state and spread out of it in a uniform manner after activation. The dot shape also makes image analysis easier and has low aspect ratio which results in minimal physical strain on the cells. Illustrated in figure 4a, the micropattern fabrication protocol begins with preparing the coverslips. To reduce defects in the coating of PLL-g-PEG-biotin and ensure even illumination of the coverslips in the printing step, the coverslips were cleaned with 70% ethyl-alcohol and then in a UV ozone cleaner. Cleaned coverslips were then coated with the PLL-g-PEG-biotin. The PLL-g-PEG-biotin coated coverslips were adhered onto the photomask using droplets of MilliQ water.

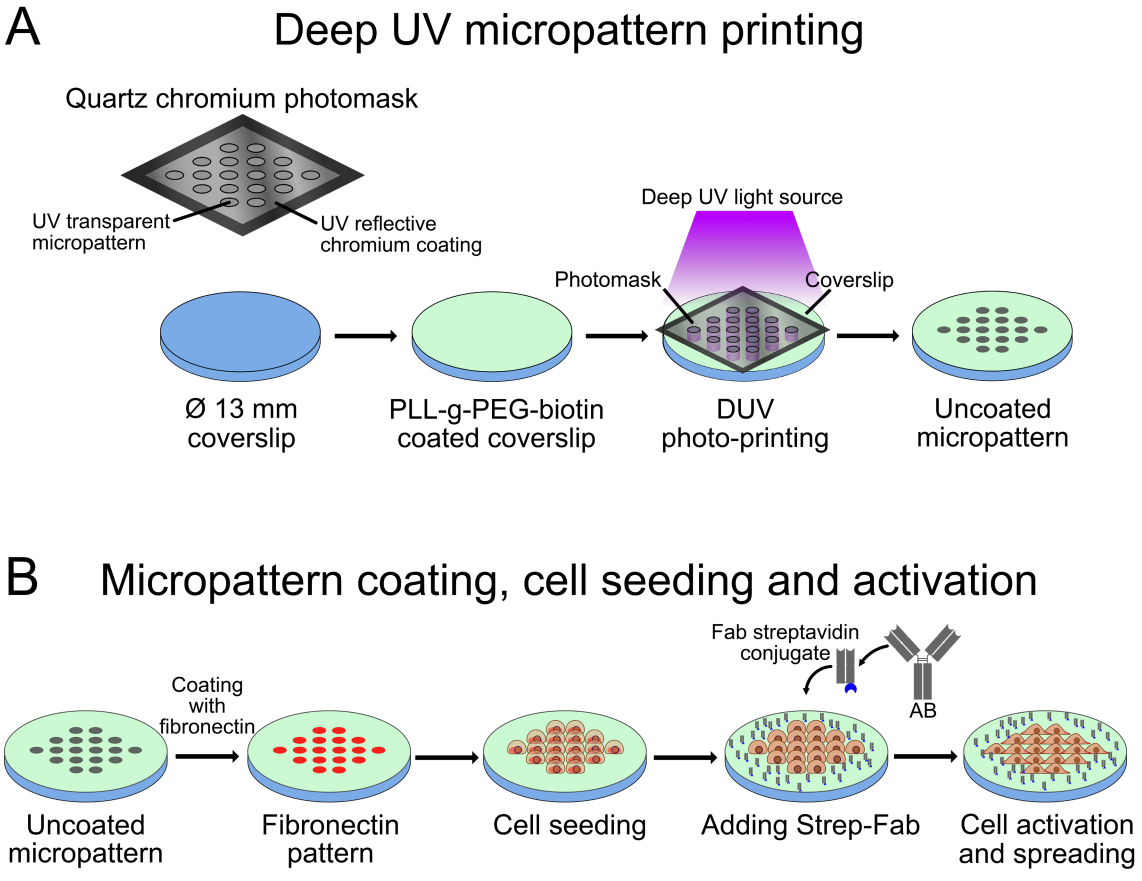

Figure 4. Illustration of dynamic micropattern preparation and activation of B cells. **A**) The micropattern printing process. A Ø 13 mm glass coverslip is coated with PLL-g-PEG-biotin and then held in in place over the photomask via surface tension of a film of water and covered by a plastic film. UV light deactivates PLL-g-PEG-biotin molecules in areas where the photomask is transparent, creating an uncoated micropattern on the surface of the coverslip. **B**) Micropattern coating and cell activation process. Coverslip with uncoated micropattern is coated with fibronectin and fibrinogen Alexa Fluor 546 solution

which binds specifically the uncoated pattern areas on the coverslip. The coverslip is then immersed in complete RPMI culturing medium into which cells are added. Cells attach on the patterned fibronectin on the coveslip surface in cell culture conditions. Excess cells are washed away and attached cells are activated with strep-α IgM Fab for 15 min in cell culture conditions. Illustrations not to scale.

The quartz chromium photomask has the micropatterns etched into the chromium layer, and these areas are transparent to UV light. When the photomask's chromium side is illuminated, the light is passed through the mask in the shape of the features etched into the chromium layer. UV light destroys the PLL-g-PEG-biotin molecules on the coverslips in the shape of this micropattern, creating a microscopic pattern of PEG free surface on the coverslip. Because of the antifouling properties of the PEG molecules, most other biomolecules do not bind or adhere to it, which makes coating the UV exposed areas of the micropattern in a second coating step straightforward (figure 4b). Cells were then seeded on the coverslips placed under culture media in a multiwell plate, and they adhered to the micropatterns via fibronectin, whereas the PLL-g-PEG-biotin molecules will repel adhesion outside the micropattern features. The PLL-g-PEG-biotin coating has a dual purpose. In addition to repelling the adhesion of cells outside the fibronectin features, it can be used as a linker for molecules ligated with streptavidin. We use this biotin-streptavidin linking to present surrogate antigen, in the form of antibody Fab fragments that are specific against the IgM BCR isotype expressed by the A20 D1.3 B cell line, on the coverslip surface neighboring the fibronectin features of the micropattern. While monovalent real epitope antigens such as hen egg lysozyme do activate B cells in solution, the BCR constant region binding Fab fragments do not. This means that we can add strep-α IgM Fab in solution to link these to the PLL-g-PEG-biotin molecules on the coverslip surface, causing surface activation of the B cells, while the same Fab-streptavidin molecules free in solution will not induce activation.

4.1 DUV micropatterning yields high quality patterning for dynamic B cell activation

4.1.1 Dynamic micropattern specificity and quality

In all experiments, after photoprinting and fibronectin coating the quality of the micropatterning was assessed by imaging the micropatterns in an epifluorescence microscope. This allowed for qualitative visual inspection of the shape, size, definition, and contrast of the patterning. Coverslips determined to have suitable micropattern quality, usually ~75% of the coverslips, were then be selected for the next steps of the experiment. To further investigate the micropattern quality in terms of specificity and functionality of PLL-g-PEG-biotin / fibronectin patterning was analyzed in an experiment where solution of strep-α IgM Fab was added on the micropatterned coverslips and then

labelled with a fluorescent secondary antibody Fab fragment against the α IgM Fab (Figure 5). The figure 5 image series shows confocal 2D images of PLL-g-PEG-biotin / fibronectin micropatterned coverslips treated with strep-α IgM Fab (figure 5a, top row) and unconjugated α IgM Fab (figure 5a, bottom row) with the fibronectin dot pattern and the PLL-g-PEG-biotin linked α IgM Fab surrounding them. The area surrounding the micropattern dots was stained with a fluorescent secondary antibody Fab only in the coverslips that had been treated with strep-α IgM Fab, and only outside fibronectin dots, confirming successful and specific anchoring of α IgM antibody Fab fragments via biotin-streptavidin link to the coverslip surface. Intensity profiles of lines intersecting the fibronectin dots, shown in figure 5b, further display the selectivity of the PLL-g-PEG-biotin and fibronectin surfaces. It is notable that while there is no meaningful overlap in the areas of fibronectin and strep-α IgM Fab, the transition area from one to the other has decrease in intensity of both stainings, visible as dark halos around fibronectin dots in the merged image (figure 5b, upper rightmost image). Whether this is the result of reduced binding of the staining agents or reduction in the number the PLL-g-PEG-biotin and fibronectin molecules themselves was not determined, however it is most likely a result of imperfect illumination of the coverslips in DUV photoprinting, creating a fall-off of illumination on the edges of the dot features, and imperfect destruction of the PEG molecules in the feature edges, corresponding to the fall-off in staining.

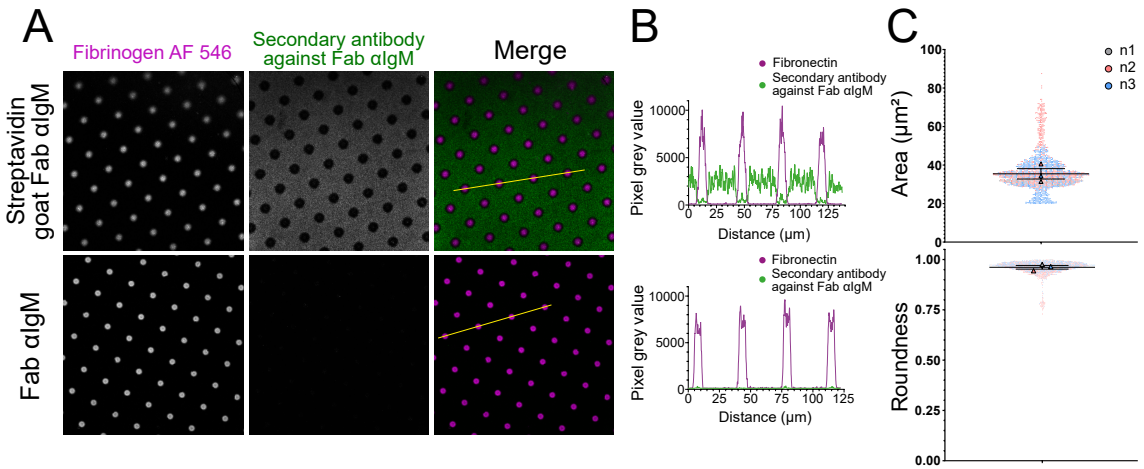

Figure 5. Micropattern coating specificity and quality of patterning. **A)** Confocal microscope images of coverslip surface with 5 μm dot pattern stained with fibrinogen AF-546, and strep-α IgM Fab (upper row) or α IgM Fab (lower row) stained with a fluorescent secondary antibody Fab fragment. **B)** Intensity profile of a line intersecting the micropattern showing the intensity of fibrinogen and fluorescent antibodies of the respective images. **C)** Pattern diameter and circularity pooled from images from three experiments (black bar: Median of all data points). Images/Number of dots measured: n1, 7/141; n2, 17/745; n3, 58/774

The confocal images were quantitatively analyzed to measure the fibronectin/fibrinogen dots for area and roundness. To do this, a dot analysis macro was created to automatically quantify the size and morphology of the patterns. Figure 5c shows that our printing method yields highly repeatable pattern shape with size of the patterns being more susceptible for batch-to-batch variation while still having consistent enough mean size for our use case. Based on the data set from three batches of coverslips with total of 1660 individual dots, the photomask with 5 μm diameter dots yields, in average, dots with a diameter of 6.8 μm. Reason for this magnification in the dot size is the thickness of the water film between the coverslip and the mask creating a space between them, which leads to enlargement of the projected image of the micropattern on the coverslip. These results show high specificity and separation of the fibronectin and PLL-g-PEG-biotin areas and consistency in the shape and size of the micropattern features.

4.1.2 Streptavidin conjugated α IgM antibody Fab fragments activate B cells seeded on dynamic micropatterns with PLL-g-PEG-biotin coating

It is well established that antibodies targeting the Fc region of BCR cause BCR signaling and B cell activation in soluble and surface bound form whereas monovalent Fab fragments of antibodies targeting the same site only cause cell activation when presented on a surface (Woodruff et al., 1967). To show that the micropatterning method is capable of activating B cells via surface presented antigen, B cells were treated with surrogate antigen in three conditions. Functionality of the strep-α IgM Fab conjugate as a surface bound antigen surrogate was tested by seeding B cells on micropatterned coverslips and activating the cells with the strep-α IgM Fab. As negative controls, micropatterned coverslips with PLL-g-PEG without biotin and coverslips treated with α IgM Fab without streptavidin with otherwise identical conditions to the experimental coverslips were tested in cell activation (Figure 6). Following the activation, cells were incubated for 15 minutes then fixed, stained with fluorescent phalloidin, DAPI, and fluorescently labelled anti-pBtk and anti-pPLCγ2 antibodies, and the coverslips were mounted for imaging. The activation of the A20 D1.3 cells was confirmed from spinning disk confocal microscopy images of the cells, taken at the coverslip surface where the cell bottom was visible. The confocal 2D images have a voxel size of 0.101x0.101x1 μm, and were manually focused to the coverslip surface, acquiring a 100 nm optical section of the cell bottom. Cell area was analyzed from the confocal images to quantify the spreading of the cells at coverslip surface. The cell, and micropattern fibronectin features were segmented from image background by automatically setting a threshold value in FIJI. Phalloidin channel was chosen for segmentation of the cell from background because it, from the acquired image channels, most accurately represents the outline of the cell. The resulting binary image of the phalloidin channel was further processed with morphological dilate and erode operations to smooth out the edges of the cell while

conserving the area made up by positive value pixels to make the cell area measurement accurate. The cell area was quantified by segmentation resulting binary image to create a ROI corresponding to the cell in the image and measuring the area of the ROI. Image series in figure 6 shows that B cells do not spread on the coverslip when cells are treated with soluble α IgM Fab without streptavidin (figure 6, top image row) or when strep-α IgM Fab is used in absence of biotin moieties on the coverslip surface (figure 6, bottom image row) leading to failure in adhesion of Fab fragments to coverslip surface. Only when strep-Fab α IgM is applied to biotinylated PLL-g-PEG coated coverslips, do the Fab fragments adhere to the coverslip and cause B cell activation and spreading over the coverslip surface (fig 6. middle row). This confirms that the strep-α IgM Fab binds to the biotinylated PLL-g-PEG on the coverslip surface and reliably causes immunological activation in this surface bound form.

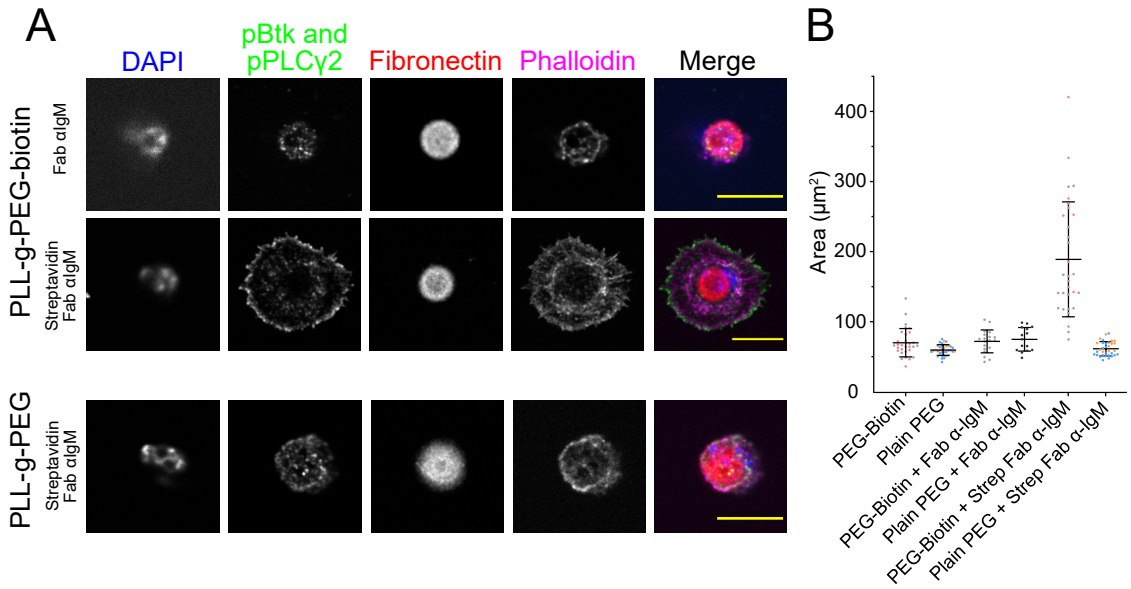

Figure 6. B cells seeded on micropatterned coverslips get activated in presence of α IgM antibody Fab fragments conjugated to streptavidin. **A**) Three conditions of cell activation were tested: 1) Cells seeded on fibronectin micropatterns on PLL-g-PEG-biotin coated coverslips and treated with α IgM Fab. 2) Cells seeded on fibronectin micropatterns on PLL-g-PEG-biotin coated coverslips and treated with strep-α IgM Fab. 3) Cells seeded on fibronectin micropatterns on PLL-g-PEG coated coverslips and treated with strep-α IgM. Cells were incubated for 15 minutes, fixed, and stained for pBtk and pPLCγ2, actin, and DNA. Confocal images of the cells were taken at the coverslip surface. **B**) Cell spreading was quantified from an area measurement from binary image of the phalloidin channel. Number of cells: PEG-biotin (N=2), 30 cells; Plain PEG (N=2), 36 cells; PEG-biot + Fab α-IgM (N=1), 19 cells; Plain PEG + Fab α-IgM (N=1), 15 cells; PEG-biot + Strep-Fab α-IgM (N=2), 31 cells; Plain PEG + Strep-Fab α-IgM (N=2), 33 cells. Bars represent mean and standard deviation.

Together the results of these two experiments show that the DUV photo-printing method produces micropatterns with reproducible quality and that the PLL-g-PEG-biotin coating effectively triggers B cell activation via surface bound antigen on an imaging compatible media.

4.2 B cells consistently get activated and spread on dynamic micropatterns

Dynamics of activation and spreading of B cells on dynamic micropatterns was further observed by fixing cells at different time points after activation. Five minutes and fifteen minutes were chosen as the fixing time points with non-activated cells as control. Fixed samples were stained, in general, for DNA, actin, and with antibodies against pBtk and pPLCγ2 with the same fluorescent label to reveal BCR signaling associated phosphorylation, then imaged with confocal spinning disk microscope. Analysis of single confocal plane images (figure 7) was done as before to measure the area of the cells at the micropatterned coverslip surface. We detected that non-activated cells largely occupy only the areas of the fibronectin features, with a ring of actin presenting the edges of the cell (figure 7a). After 5 minutes of activation, a B cells (figure 7a) show expansion outwards from the fibronectin dot. Cells fixed after 15 minutes of activation have spread over more area and protrusive actin structures have developed (figure 7a). Somewhat scattered clusters of Btk and PLCγ2 activity is seen in non-activated cells. The Btk and PLCγ2 activity is typically enriched near to the cell edges in cells fixed after 5 minutes of activation, and cells fixed after 15 minutes of activation show clear majority of the Btk and PLCγ2 activity enriched in the leading edge (figure 7a). Seen in figure 7b, the cell area data reveals repeatable and consistent cell spreading during 15 minutes of activation. It’s important to emphasize that mean values of each replicate experiment were used to calculate P-values instead of using each cell as N. This was done to compare the conditions weighted by the number of experiment repetitions and not by the number of cells in each condition.

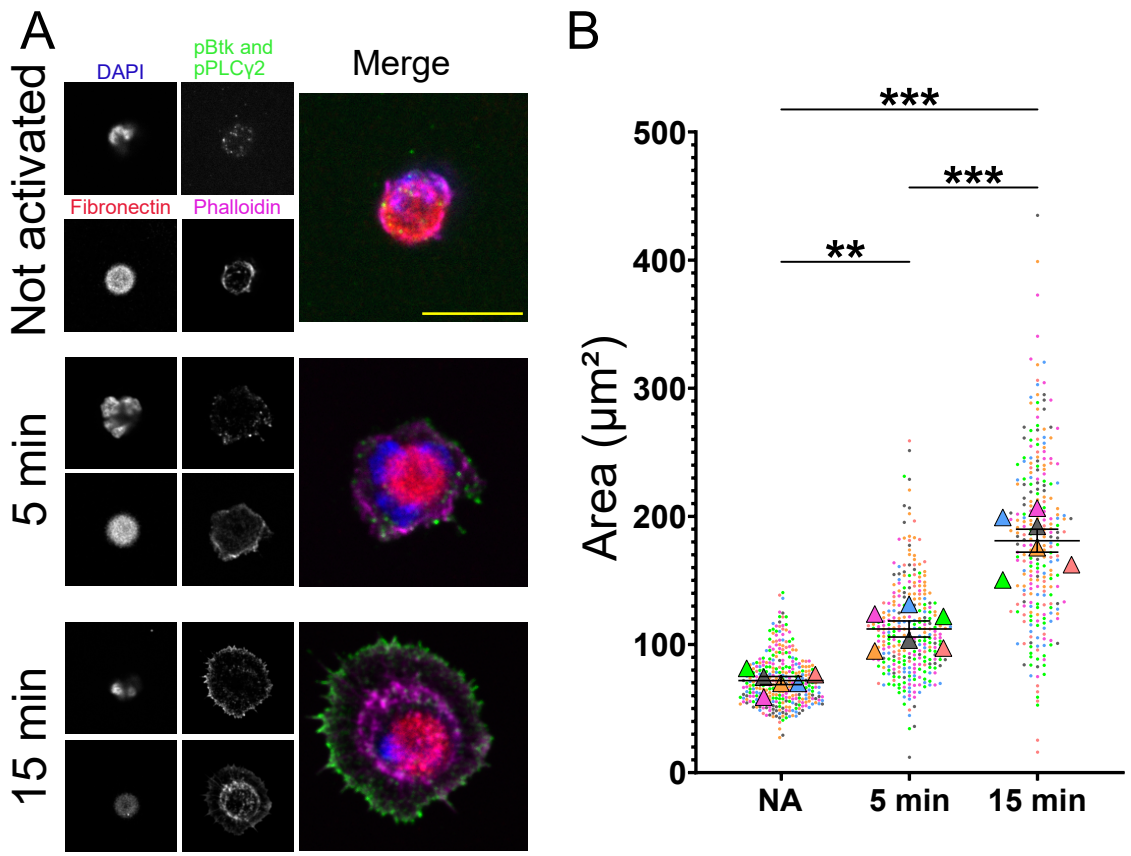

Figure 7. **A**) Representative images of the coverslip surface with B cells seeded on top of dynamic micropatterns, fixed without activation, after 5 minutes, and after 15 minutes of activation and stained for DNA, pBtk+pPLCγ2 and actin. **B**) Cell area at the coverslip surface measured using image measurement macro (3.6.2) from the images of B cells. Each cells value is represented as a dot, with the color corresponding to the experiment that the cell was part of. Mean values of all cells in each experiment are shown as triangles with their experiment respective color. Average of all the mean values of repetition experiments, with standard deviation, are shown as black bars in front of the data points. Black bars and asterisks on top of the graph show significance of the p-values from paired Student's T-test between mean values of different time points, yielding N of 6. Number of cells: NA, 73, 74, 80, 49, 25, 39; 5 min, 58, 74, 66, 41, 31, 37; 15 min, 47, 49, 57, 34, 33, 37. * < 0.05, ** < 0.01, *** < 0.005, **** < 0.001.

4.3 Image analysis pipeline

Multiple ImageJ macro scripts were written to automate laborious parts of the image analysis pipeline. Hundreds of images were taken during the course of the project with many images containing multiple cells, meaning that for quantification of this amount of image data some amount of automation was necessary.

The details of image segmentation and measurement are described in the Materials and Methods. Three macros were written to aid in the analysis of single plane confocal images of cells on micropatterns. These macros were used to: 1) Covert and save the images in TIFF format, 2) Crop images to contain only one cell per image, 3) Analyze

the cropped images to measure shape and fluorescence intensity of the cell outside and inside the micropattern. These three macros are referred to as: file conversion macro (figure 8a), image cropping macro (figure 8b), and image measurement macro (figure 9), respectively. The image cropping macro was created to simplify the analysis of wider field of view images containing multiple cells (figure 8b). The image cropping macro automates some parts image cropping, greatly accelerating the work. The image measurement macro was created to analyze intensity of actin, and activated Btk and PLCγ2, in the parts of the plane of cell adhesion that were outside and inside the micropattern. The image measurement macro uses same image segmentation methods used in the analysis of micropattern quality (4.1.) for its segmentation functionality (figure 9). The image measurement macro creates a third ROI for the image that contains only the part of the cell outside the micropattern by subtracting the pattern ROI from the cell ROI (figure 9). Signal intensities inside the three ROIs would then be analyzed in all channels, as well as the shape descriptors and size of the ROIs.

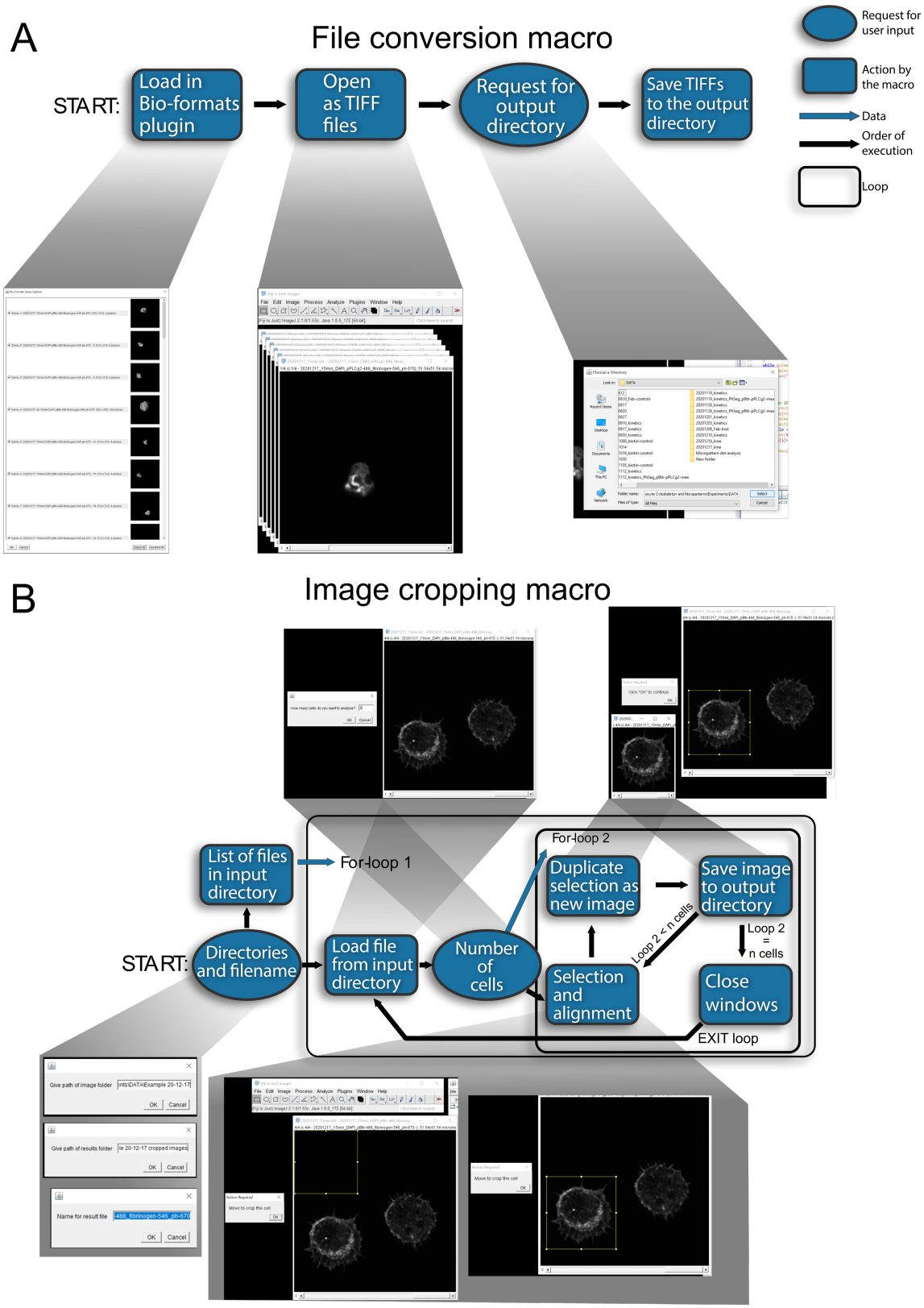

Figure 8. Flow-chart illustration of the ImageJ macros for converting of microscope file-formats and cropping images to contain one cell per image file. **A**) The file conversion macro needs manual opening of images. After a set of images has been opened on ImageJ, the macro can be run. The macro will first request the user to specify a directory for the saved images and will then save the images individually to the given directory. **B**) The image cropping macro will duplicate and crop images with the help by the user. It

asks the user for an input and output directories and automatically loads images from the input directory. The macro asks the user to identify how many cells there are and where the cells are positioned in the image and then duplicates the image in user-selected area, effectively creating a cropped copy of the image containing the cell. The cropped images are then automatically saved in the output directory.

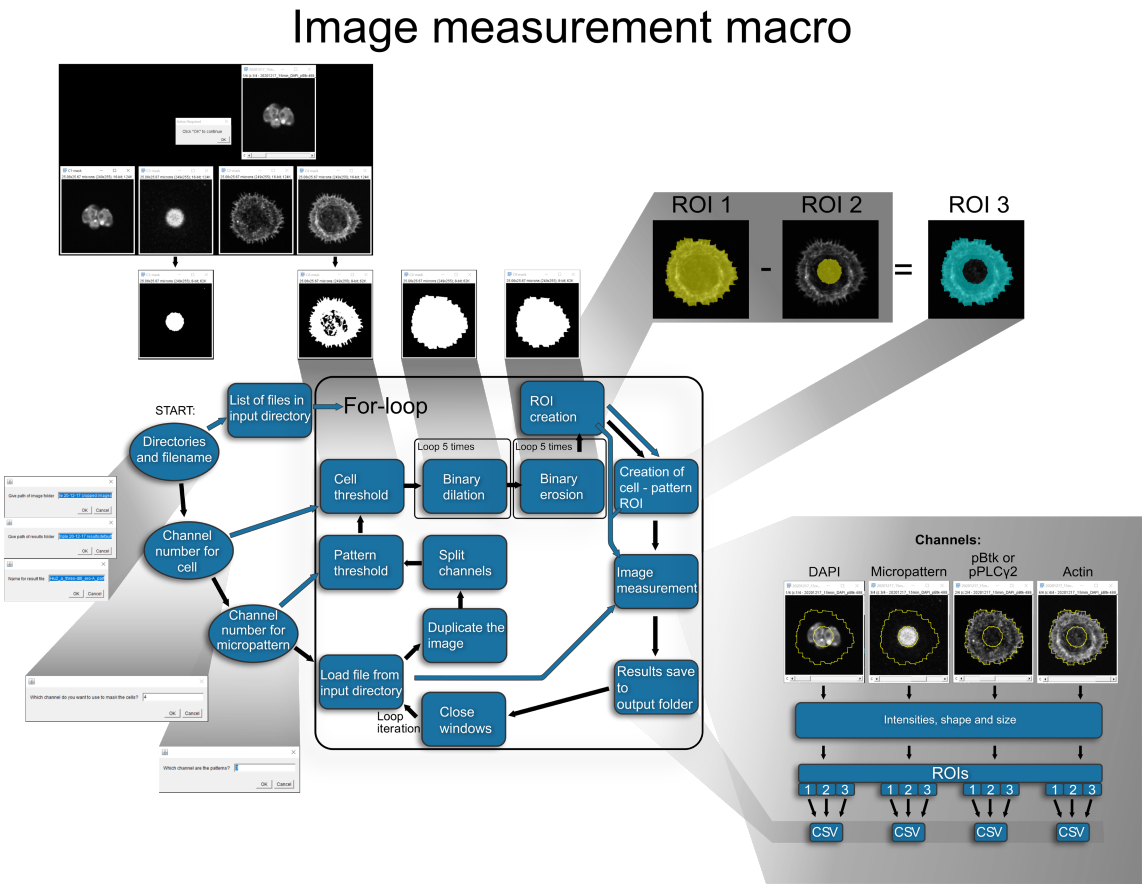

Figure 9. Flow-chart illustration of image measurement macro for ImageJ that is used to analyze the images generated by the image cropping macro of figure 8b. The macro starts by asking the user to specify input and output directories and the channel numbers of actin and micropattern channels, and in addition asking the user to type a name to be used as a template for the results files. The macro then opens an image from the input folder and does image segmentation on the actin and micropattern channels and creates three regions of interest (ROIs) representing the cell and parts of the cell inside and outside of the micropattern. Intensities inside the ROIs are then analyzed in all channels and the results are saved in the output folder, which is followed by opening the next image from the input folder, starting the analysis process again.

4.4 Analysis of Btk and PLCγ2 intensities of B cells upon activation on micropatterns

Upon BCR activation, signaling proteins Btk and PLCγ2 are phosphorylated as part of signaling pathways leading to B cell activation (Harwood and Batista, 2010; Wen et al.,

2019). To observe the activation of the BCR signaling pathways, fixed samples of B cells activated on dynamic micropatterns were stained with fluorescently labeled antibodies against phosphorylated Btk or PLCγ2. The samples were imaged at the plane of adhesion with spinning disk confocal microscope and the intensity of fluorescent light was measured from the images (figure 10a). Since the antibodies for pBtk and PLCγ2 had the same fluorescent label, they were used in separate samples.

Images were first converted to TIFF with the file conversion macro and then cropped with the image cropping macro (figure 8a, 8b). Image measurement macro was used to segment the images to ROIs representing the area inside and outside the micropattern and area of the whole cell, to compare the fluorescence intensities in these areas (figure 9).

To assess the overall activation of pBtk and pPLCγ2 in the cells, mean intensity was measured inside the cell, spreading, and pattern ROIs. Seen in figure 10b, are the mean intensities measured for each cell from each region of interest. Unactivated cells show low mean intensities across all ROIs for both pBtk and pPLCγ2 compared to mean intensities in samples fixed after five and fifteen minutes of activation. Change in the mean intensities between five minute and fifteen-minute data shows no statistical significance. It is important to mention that the average of the intensity values in a repetition were used as data points in the Student's T-test. This was done to represent one repetition of the whole experiment as a single sample in the statistical analysis instead of using single cells as sample points.

The average mean intensities of pPLCγ2 in the cells were at similar levels in all ROIs at 5 minutes and 15 minutes after activation in each replicate experiment (figure 10b). Two replicate experiments have very low mean intensities compared to the rest, suggesting that the cells may not have activated properly in those experiments.

Because of the selective binding of anti-BCR strep-Fab only outside the fibronectin pattern and at the surface of the coverslip, BCR activation and the highest localization of the activated BCR signaling proteins is anticipated to happen outside the pattern. To test this hypothesis, mean intensity outside and inside the fibronectin pattern was compared in samples fixed without activation and after five and fifteen minutes (figure 10c). For each cell, the mean intensity outside the fibronectin pattern was divided with mean intensity inside the pattern to create a ratio of average outside/inside intensity. Ratios above one mean higher enrichment of protein activity outside the fibronectin dot and ratios lower than one mean higher enrichment inside the fibronectin dot (figure 10c). The results show that both pBtk and pPLCγ2 have ratios less than one when not activated. This is expected, since the area outside the fibronectin pattern in cells that are not activated is very small and contains only the very edge of the cell. Samples fixed after five minutes of activation show consistently higher ratios, though with a high variability

between repetitions making change from unactivated statistically insignificant. In the case of pBtk, the difference in the ratios from unactivated cells to those fixed after fifteen minutes of activation is highly significant, however. Seen in figure 10c, in the five-minute and fifteen-minute activations pBtk has higher enrichment outside the dot pattern compared to pPLCγ2, with difference in fifteen-minute activation being statistically significant. This difference seen in the quantification is likely due to the differences in the distribution of the signal in pPLCγ2 and pBtk. pBtk is quite evenly distributed in the leading edge and seems to correlate with actin structures, whereas pPLCγ2 distributed in clusters in the leading edge and inside the cell bottom.

Actin cytoskeleton is engaged to spread the cell after activation and has important roles in IS formation and function. Therefore, fluorescence intensity of phalloidin was also analyzed from the same images to see if actin also enriches outside the micropattern (figures 10c). Actin shows slightly increasing ratios after five and fifteen minute activation when compared to non-activated samples but this change is not enough to be statistically significant. While not significant, the data suggests some temporal and spatial enrichment of actin with the Btk and pPLCγ2 signaling proteins outside the micropattern, and their simultaneous engagement in B cell activation. This observation supports the established notion that actin cytoskeleton is engaged in cell spreading and B cell signaling.

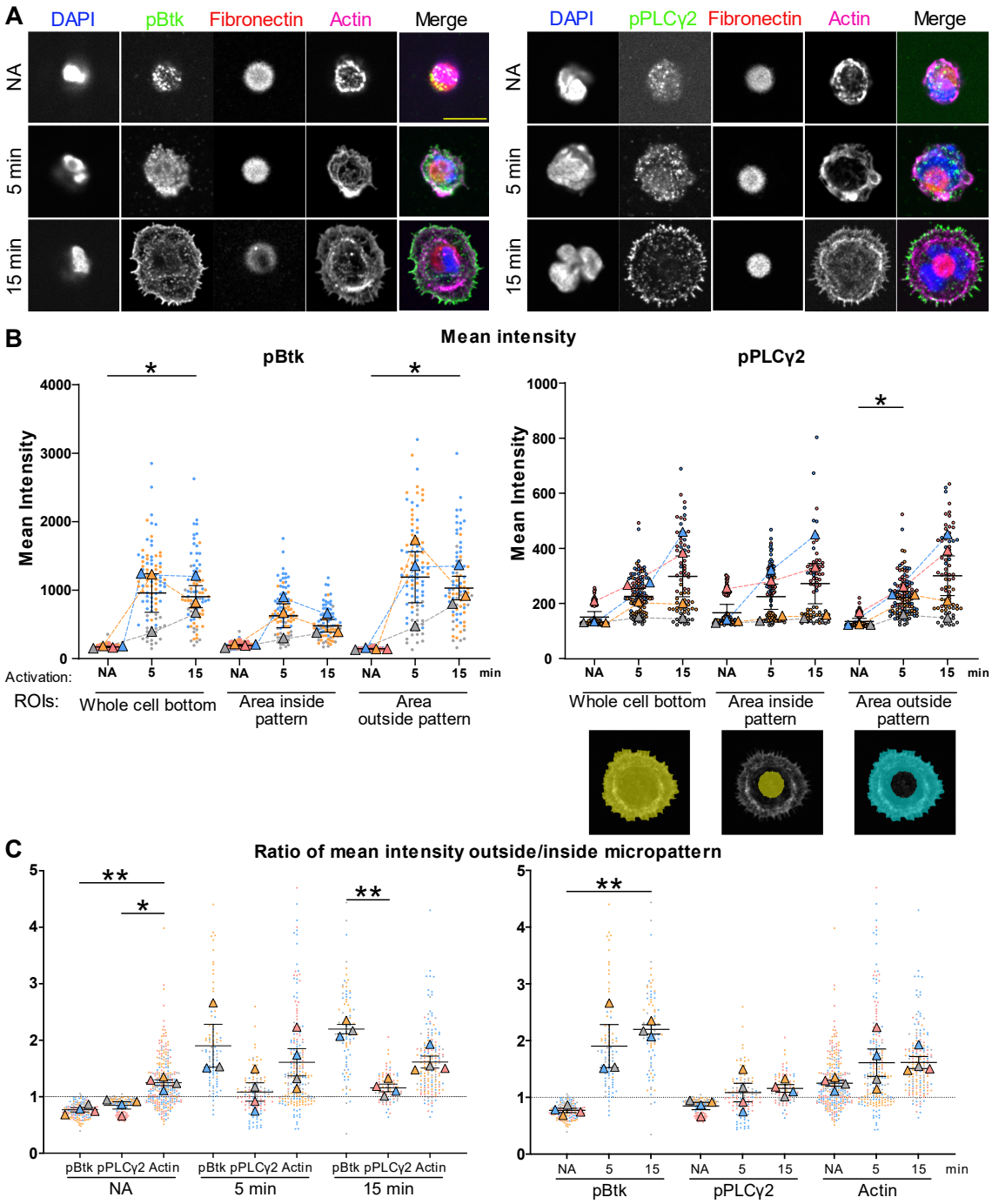

Figure 10. Analysis of Btk and PLCγ2 activity and enrichment in B cells on micropatterns during activation. **A**) Representative images of fixed B cells imaged with spinning disk confocal microscope. B cells were fixed without, 5, and 15 minutes after activation and stained for DNA, and pBtk or pPLCγ2. Scale bar = 10 μm. **B**) Mean intensity of pBtk and pPLCγ2 measured from samples represented in A. The cells were segmented into ROIs and intensities were measured inside these ROIs. **C**) The ratio of mean intensities outside fibronectin pattern to mean intensity inside fibronectin pattern in three fixing timepoints after activation for pBtk, pPLCγ2 and actin. In all graphs, each dot represents a cell, and each color represents replicate experiment. Mean value of all cells in a replicate experiment is shown as a colored triangle. Error bars represent mean and standard error of the mean. An average of all cells in a replicate experiment was used

as a single number in student's t-test, yielding an N of 4 for all conditions except 5 and 15 minutes with pBtk staining where N is 3. Number of cells: NA pBtk, 22, 43, 38, 38; NA pPLCγ2, 27, 37, 36, 35; NA Actin, 49, 80, 74, 73; 5 min pBtk, 20, 42, 32; 5 min pPLCγ2, 21, 35, 32, 26; 5 min Actin, 41, 35, 74, 58; 15 min pBtk, 19, 39, 28; 15 min pPLCγ2, 15, 33, 10, 19; 15 min Actin, 34, 33, 49, 47. * < 0.05, ** < 0.01, *** < 0.005, **** < 0.001.

4.5 Live imaging and Airyscan imaging

Live imaging study was conducted to test the live-imaging compatibility of our micropatterning system. Largest change in the experimental methodology required by live imaging was the change of coverslip mounting from a microscope slide of the fixed samples to an imaging chamber with a hole on the bottom. This meant that each coverslip had to be attached by hand to the imaging chamber, lengthening the sample preparation time and this among other things resulted in fewer samples. Activation solution, same as with the fixed samples, would activate all the cells at the coverslip at the same time but only a few cells, ones that would fit the field-of-view selected, could be imaged from beginning to the end of the activation event.

For this study, the cells were transfected with a plasmid containing a cDNA encoding for LifeAct fluorophore which stains the actin. B cells were then seeded to the coverslips as before. The coverslips were then attached onto the bottom of confocal imaging dishes via melted Parafilm. The confocal dishes were kept inside an environment chamber during imaging and activation of cells was done in the dish after putting it on the microscope stage. Only the actin channel was acquired in real-time experiment since this would speed up the acquisition, and since the fibronectin patterning is static and cells were not anticipated to migrate from their fibronectin dot it would not be imperative to acquire the fibrinogen channel in all time steps. Both lower frequency 0.1 Hz and higher frequency 1 Hz image sequences were captured with longer and shorter acquisition lengths, respectively. Lower frequency imaging captured the cell activation and spreading for 10-15 minutes (figure 11a). Higher frequency imaging (data not shown) was conducted after the 10-15 minutes of lower frequency imaging on different cells on the same coverslip to observe faster actin dynamics not visible in the lower frequency imaging. High frequency captures revealed actin retrograde flow and protruding of filopodia over 10 seconds of acquisition. Since the rigidity of glass coverslip doesn't allow for antigen internalization and cell contraction these phenomena could not be observed and longer live image acquisitions were not conducted at any acquisition frequency.

The live imaging shows that dynamic immunological activation of B cells seeded on micropatterns could be monitored in real time. The live imaging of actin shows that the activation on live seeded cells is similar to the fixed samples but shows it with higher temporal definition. Filopodia can be seen jetting outwards from the fibronectin confined dot within the first minutes (white arrows figure 11A), followed by the formation of

lamellipodia as the cell spreads across coverslip surface (yellow arrows figure 11A). The cells achieve their final size of spreading after about 10 minutes.

Airyscan confocal imaging was conducted on a sample of B cells fixed after 15 minutes of activation, produced as before, to test super-resolution imaging of micropatterned B cells. Only actin channel was acquired due to time constraints. The Airyscan imaging system produced z-stack images with voxel size of 0.0553 x 0.0553 x 0.2243 µm. Representative image shows fine actin structures visible in the single xy section of the cell bottom (figure 11b). The increased spatial resolution of the Airyscan microscope compared to the spinning disk confocal microscope resolves small actin structures of the cell with higher definition. For example, protruding actin structures can be discerned form the background actin structures inside the cell whereas in spinning disk confocal microscopy images these structures are harder to distinguish. The increased resolution could open further possibilities for analyzing the organization of actin structures and colocalization of BCR signaling components upon B cell activation. XZ and YZ cross sections show the cell body in the middle, with height of 6.3 µm, and the leading edge of the cell at the resolution limit with height ~1 µm (figure 11b).

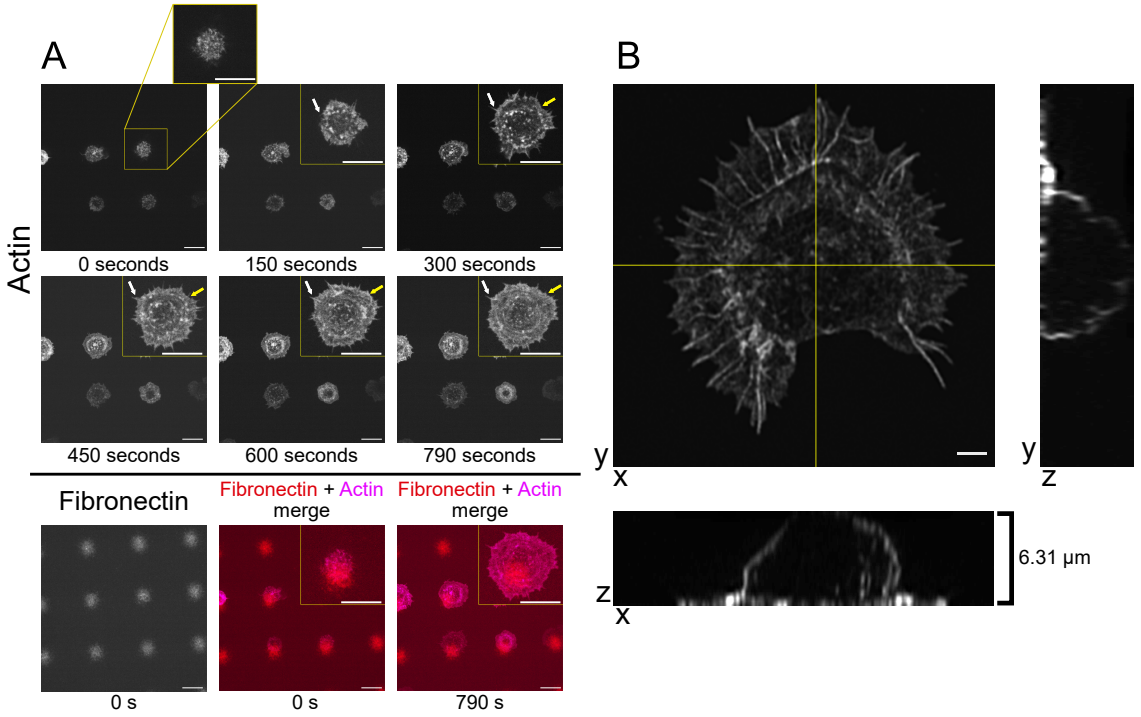

Figure *11*. Representative spinning disk confocal microscopy images of live B cells and Airyscan confocal super-resolution microscopy images of fixed B cells on micropatterns. **A**) Sequence of representative images from a live confocal spinning disk microscopy acquisition of B cell activation on a fibronectin micropattern, acquired at 0.1 Hz framerate. Activation happens approximately 10-20s after the start of image acquisition. Only a single frame of the fibronectin channel was acquired at the beginning of the live-cell imaging to speed up acquisition. Image insets have one cell

magnified. White arrows mark an example of a growing filopodium. Yellow arrows mark an example of an area where cell lamellipodia expand as the cell spreads. Scale-bar = 10 µm. **B**) Representative images from an Airyscan confocal image stack of a B cell, fixed 15 minutes after activation. XY image is a single optical section at the coverslip surface. Yellow lines on YX image indicate the cross-sections from which YZ and ZX projections are created. Scale-bar = 2 µm.

5. DISCUSSION

The DUV micropatterning technique yielded consistent quality of micropatterned coverslips with ~75% of all printed coverslips having good micropatterns. While demanding in terms of precision of manual handwork, the DUV micropattern printing protocol is less prone to variation since it is essentially a physicochemical process, compared to perhaps the most time-consuming part of the project, which was the optimization of cell seeding. Higher number of cells adhering to the micropatterns and stronger adhesion to the fibronectin features micropattern would yield higher number of cells to image and produce higher consistency in the conditions of the cells before activation. While cell adhesion and alignment with the micropattern was adequate for this study, further studies would benefit from improvement in these areas. In this study ~200 000 cells were applied to a well per coverslip, yet not all the fibronectin dots got occupied with a cell. In fact, sometimes the cells hardly attach at all, and are washed away with culturing medium. During the cell seeding protocol the cells' environment changes as they are transferred from ideal environment of the cell incubator into test tube and then to a multiwell plate in room temperature. This, in addition to washing the coverslips with room- and even lower temperature culturing medium to remove non-adhered cells and cells adhered outside fibronectin, puts the cells under considerable stress before return to incubation for cell adhesion. Even when performing the protocol same way every time, the number of adhered cells would vary. It is quite hard to discern whether the variation in the number of cells adhered on the micropattern and the strength of this adhesion to fibronectin is mainly caused by the quality of the patterned substrate, the condition of the cells, or some other factor. While monitoring of the adhesion process was conducted, via conventional bright field microscope, it revealed only crude information of the micropattern adhesion because of the limitations of the microscope, mainly the inability to see the micropatterns. And while it was possible to look for the patterned adhesion of cells, it was impossible at that stage to know if the cells would be aligned with the actual micropatterned substrate instead of being uniformly drifted away from the pattern. The proper alignment of cells would only possibly be confirmed via fluorescence microscopy, which was impractical in the cell culture setting. Because of

this, proper alignment and activation of the cells could only be viewed after sample preparation, at the microscope, at least in fixed sample experiments. This means that one can only know about the quality of cell seeding after sample preparation. Better tools to monitor cell adhesion would help in further optimization of the cell seeding protocol and could improve consistency of samples.

In live-imaging experiments, another problem would occur because of the inconsistency in cell activation. In fact, in both fixed and living micropatterned cells, the activation with strep-α IgM Fab would not activate all B cells uniformly. Even though the mean size of B cells would get consistently larger with longer activation times, the cells had variability in their size, illustrated in figure 7b, which may be caused by variance in cell health. In live imaging, where ideally only one cell would be imaged per activation over the whole coverslip to make image acquisition as fast as possible and keep photobleaching at minimum, one would have to make tens of sample replicates to attain useful amount of data for statistical significance. However, since all cells are essentially uniform in their morphology on the patterns before activation, the cells could be selected for imaging without visual bias.

In fixed sample imaging, one challenge is the lack of automation in selection of cells for imaging. With hundreds or thousands of cells per coverslip, imaging all cells would have been impractical in terms of time and amount of data. Tens of cells would be manually selected to be imaged per condition in a single experiment. This means that the images are subjected to a selection bias by the researcher, even if conscious effort to challenge confirmation bias was exercised when selecting cells for activation. Automation of the image acquisition pipeline would have greatly improved the speed of imaging, the number of images gathered and diminish the bias in cell selection, yielding higher statistical powers. Even still, setting up an automated imaging pipeline would have been time consuming and may have created additional challenges and was therefore not worthwhile for a study of this size.

Image analysis presents many challenges for a researcher. Quantitative analysis always involves selection, categorization, or modification of the raw image data. Depending on what kind of phenomenon is observed, some part of the raw data is ignored, and other parts of the data are selected for measurement. In my study on the dynamic micropatterns and BCR signaling, the areas of interest are the physical area that the B cells occupy and the enrichment of certain active BCR signaling proteins and actin in the plane of adhesion to the coverslip. This means that two different characteristics, physical and biochemical, of the cells need to be quantified. To do quantification of physical area of the cell bottom from an image stained to show molecules within the cell is not optimal but is sufficient for this study.

There is a myriad of technologies and approaches, from simple convolution filters, like gaussian blur, to cutting-edge and complex neural networks, to process microscopy images, and depending on the quality and type of imaging any number of these can be used. For this project the technologies used in image analysis were consciously selected to be common and well known, necessitated by the timeframe of the project and the amount time allocated for learning new techniques since the bulk of the work would be in optimizing the dynamic micropatterns and gathering experimental data. Measurements of cell spreading area were done from the images of phalloidin channel, since actin is quite evenly distributed in the cell at the plane of adhesion to the coverslip and, since with the limited number of channels available, there was no room for a plasma membrane staining which possibly could have made cell outlining easier and more accurate. Since actin is not perfect for masking of the cell bottom, after setting a threshold additional processing of the binary image was done by expanding and dilating it to remove the uneven edges of the cell mask. This means that the exact numbers of the cell area may not be the most accurate, but since all images were processed in an identical manner the relative differences between the experimental conditions should be accurate. This of course presupposes that F-actin structure and quality of the phalloidin staining are consistent across all conditions, which was not controlled for. Automated parts of the image analysis pipeline were inflexible for the types of images it could analyze. The image analysis macro requires some overlap of the phalloidin ROI with the fibronectin dot ROI to work. In addition, only one cell and dot can occupy an image since the macro used here could not distinguish between more than two different ROIs when performing subtraction to create the cell minus dot ROI. Ability to keep track of different cells and their ROIs along with ability to detect ROI overlap would have greatly simplified and sped up the image analysis.

Statistical analysis of the quantified image data was done with experimental reproducibility rather than cell-level variability in mind. Instead of calculating P-values with individual cells as *n,* mean value of all cells in one condition of a repetition was used as *n*. The mean values were overlayed on top of the individual cell values in a figure, along with an error bar representing the mean and standard error of the mean of all repetitions, to create a SuperPlot (Lord et al., 2020) (figure 10). The downside of using this method of statistical analysis in our study is that, since different experimental conditions had differing numbers of cells imaged, all mean values are not calculated from the same number of individual cells and thus some mean values may not present reality as accurately as others. When analyzing some variables, the experimental variability is very high. For example, the mean intensity of pPLCγ2 showed P-values less than 0.05, considered significant, in only one comparison, which was NA cells vs 5 min activated cells for the ROI outside the micropattern (figure 10a). Comparison of the ratio of

intensities inside and outside ROIs at different time points showed similar high experimental variability (figure 10c).

There are a couple of possible sources of error in the pBtk and pPLCγ2 analysis. As shown in the results of pattern quality (4.1.1), the size of the fibronectin dots varies meaning that the relative size of the dot to the cell also varies throughout the data set. What also varies from cell-to-cell is the relative positioning of the cell with regards to the fibronectin dot. I non-activated cells this variation does not manifest fibronectin dot fills the whole cell at the adhesion site. In contrast, in the activated cells the position of the fibronectin dot can be in some other place than center of the cell. In one cell the fibronectin dot can be at the center and in another near the leading edge of the cell. The size and relative position of the fibronectin dots likely adds some inconsistency to the data. On the other hand, the variability of relative fibronectin dot location may eliminate bias towards a specific part of the cell bottom. Another matter is the organization of the pBtk and pPLCγ2 within the ROIs used in the analysis and within the cell at the plane of adhesion in general, which varied between coverslips. In some of the acquired images one can see that the signal is clearly concentrated on the leading edge of the cell while in others the signal is more scattered within the cell bottom. The organization and distribution of the signal inside ROIs is not accounted for in the comparison of mean intensities across the different ROIs because here we compare single values against each other. The phospho-antibodies used exhibited some unspecific binding to fibronectin causing a faint increase in the pBtk and pPLCγ2 channels' signal in the pattern. This signal seems to be constant across the samples but is lesser in activated cells and therefore skews the inside pattern outside pattern ratio in data points. There was variability across the replicates (figure 10B and C). This variability can be the result of difference in the amount of sample bleaching during imaging, difference in the activation environment as the amount of time spent seeding the cells varied. Adding to that, the viability of the cells changed during the study and new batches of cells were thawed every 1-2 months to get optimal attachment on the micropatterns.

The analysis of mean intensities in the three ROIs gives a rough estimate of enrichment of the signaling proteins and cannot be considered to measure localization of the signaling clusters. The analysis performed here does not capture the full complexity of receptor clustering and signaling dynamics but instead showcases the general enrichment of Btk and PLCγ2 activity in the context of novel activation method which are the dynamic micropatterns.

6. CONCLUSIONS

Micropatterning is a term that encompasses varied assortment of techniques with equally varied biological applications. Most of these techniques have seen preliminary use in proof-of-concept methodological papers or engineering studies and have not yet been established into the biologists' toolsets. Even still, these methods that allow tighter control and higher complexity of the mechanical and chemical environment of cells and molecules in artificial setting can be the logical next step for in vitro experiments as scientific inquiry expands from single cells on passive isotropic substrates to more dynamic and higher order systems of cells and extracellular environments. Although not observing any higher order cell-to-cell phenomena in this study, our dynamic micropatterns provide a point of entry for new studies of immunological activation of lymphocytes by controlling the area and timing of activation via specific anchoring of soluble antigen to patterned biotin after cell adhesion. The greatest advantage of this method is that it allows monitoring the surface presented antigen induced cell activation from the very beginning with high resolution imaging techniques. Further, we demonstrate the monitoring of key signaling proteins associated with cell activation and show interesting image analysis possibilities enabled by the fluorescent labelling of the micropatterns. We show that the enrichment of both pBtk and pPLCγ2 in the plane of cell adhesion correlates with the areas of the surrogate antigen strep-α IgM Fab on the coverslip, confirming the hypothesis that these signaling proteins enrich near areas of antigen engagement in the cell. We also demonstrate the compatibility of dynamic micropatterns with live cell imaging and super-resolution imaging which makes it possible to both expand and narrow the observation of intracellular processes of B cell activation. Chiefly, this study showcases the power of the dynamic micropattern method as a tool for further inquiry. In the future, higher spatial and temporal resolution imaging of early events of B cell activation on dynamic micropatterns would be intriguing and could further illuminate the interaction of actin, BCR-antigen complex and the immediate signaling proteins.

7. Acknowledgements

I want to acknowledge:
Pieta K. Mattila for her guidance, support and insight into the scientific process of writing the thesis
Sara Hernández Perez for her unwavering determination and help in the lab and support and insight in the analysis of the experimental data
All members of the Lymphocyte Cytoskeleton Group for their support in and out of lab and for their inclusion to the group
The Cell Imaging and Cytometry (CIC) Core for vital training, help and access to the microscopy facilities.
Turku BioImaging MSc programme for the privilege and opportunity to learn and succeed in my studies.
My friends and family for their trust and compassion in my steps towards success in my studies.

8. References

Abbas, A.K., A.H. Lichtman, and S. Pillai. 2021. Cellular and Molecular Immunology E-Book 10th Edition. Elsevier Limited (UK). London: Elsevier Limited (UK). VBID: 9780323757508. https://clinicalkeymeded.elsevier.com/books/9780323757508.

Adler, L.N., W. Jiang, K. Bhamidipati, M. Millican, C. Macaubas, S. chen Hung, and E.D. Mellins. 2017. The other function: Class II-restricted antigen presentation by B cells. *Frontiers in Immunology*. 8:1–14. doi:10.3389/fimmu.2017.00319.

Amin, R.H., and M.S. Schlissel. 2008. Foxo1 directly regulates the transcription of recombination-activating genes during B cell development. *Nature Immunology*. 9:613–622. doi:10.1038/ni.1612.

Arana, E., A. Vehlow, N.E. Harwood, E. Vigorito, R. Henderson, M. Turner, V.L.L.J. Tybulewicz, and F.D. Batista. 2008. Activation of the Small GTPase Rac2 via the B Cell Receptor Regulates B Cell Adhesion and Immunological-Synapse Formation. *Immunity*. 28:88–99. doi:10.1016/j.immuni.2007.12.003.

Avalos, A.M., and H.L. Ploegh. 2014. Early BCR events and antigen capture, processing, and loading on MHC class II on B cells. *Frontiers in Immunology*. 5:1–5. doi:10.3389/fimmu.2014.00092.

Batista, F.D., and M.S. Neuberger. 2000. B cells extract and present immobilized antigen: implications for affinity discrimination. *The EMBO journal*. 19:513–520. doi:10.1093/emboj/19.4.513.

Berland, R., and H.H. Wortis. 2003. Normal B-1a cell development requires B cell-intrinsic NFATc1 activity. *Proceedings of the National Academy of Sciences of the United States of America*. 100:13459–13464. doi:10.1073/pnas.2233620100.

Bezanilla, M., A.S. Gladfelter, D.R. Kovar, and W.L. Lee. 2015. Cytoskeletal dynamics: A view from the membrane. *Journal of Cell Biology*. 209:329–337. doi:10.1083/jcb.201502062.

Brezski, R.J., and J.G. Monroe. 2007. B Cell Antigen Receptor-Induced Rac1 Activation and Rac1-Dependent Spreading Are Impaired in Transitional Immature B Cells Due to Levels of Membrane Cholesterol. *The Journal of Immunology*. 179:4464–4472. doi:10.4049/jimmunol.179.7.4464.

Burbage, M., S.J. Keppler, F. Gasparrini, N. Martínez-Martín, M. Gaya, C. Feest, M.C. Domart, C. Brakebusch, L. Collinson, A. Bruckbauer, and F.D. Batista. 2015. Cdc42 is a key regulator of b cell differentiation and is required for antiviral humoral immunity. *Journal of Experimental Medicine*. 212:53–72. doi:10.1084/jem.20141143.

Carpi, N., M. Piel, A. Azioune, and J. Fink. 2011. Micropatterning on glass with deep UV. *Protocol Exchange*. doi:10.1038/protex.2011.238.

Chiou, P.Y., A.T. Ohta, and M.C. Wu. 2005. Massively parallel manipulation of single cells and microparticles using optical images. *Nature*. 436:370–372. doi:10.1038/nature03831.

Davies, D.R., and H. Metzger. 1983. Structural basis of antibody function. *Annual review of immunology*. 1:87–117. doi:10.1146/annurev.iy.01.040183.000511.

Davies, D.R., E.A. Padlan, and S. Sheriff. 1990. ANTIBODY-ANTIGEN COMPLEXES. *Annual Review of Biochemistry*. 59:439–473. doi:10.1146/annurev.bi.59.070190.002255.

Dusseiller, M.R., D. Schlaepfer, M. Koch, R. Kroschewski, and M. Textor. 2005. An inverted microcontact printing method on topographically structured polystyrene chips for arrayed micro-3-D culturing of single cells. *Biomaterials*. 26:5917–5925. doi:10.1016/j.biomaterials.2005.02.032.

Feng, Y., Y. Wang, S. Zhang, K. Haneef, and W. Liu. 2020. Structural and immunogenomic insights into B-cell receptor activation. *Journal of Genetics and Genomics*. 47:27–35. doi:10.1016/j.jgg.2019.12.003.

Fleire, S.J., J.P. Goldman, Y.R. Carrasco, M. Weber, D. Bray, and F.D. Batista. 2006. B cell ligand discrimination through a spreading and contraction response. *Science*. 312:738–741. doi:10.1126/science.1123940.

Harwood, N.E., and F.D. Batista. 2010. Early events in B cell activation. *Annual Review of Immunology*. 28:185–210. doi:10.1146/annurev-immunol-030409-101216.
Heasman, S.J., and A.J. Ridley. 2008. Mammalian Rho GTPases: new insights into their functions from in vivo studies. *Nature Reviews Molecular Cell Biology*. 9:690–701. doi:10.1038/nrm2476.
Kim, J.J., K.W. Bong, D. Irimia, S. Patrick, M.G. Hospital, B. Engineering, S. Korea, and G. Hospital. 2017. HHS Public Access. 16:139–146. doi:10.1038/nmat4747.Porous.
Kläsener, K., P.C. Maity, E. Hobeika, J. Yang, and M. Reth. 2014. B cell activation involves nanoscale receptor reorganizations and inside-out signaling by Syk. *eLife*. 3:e02069. doi:10.7554/eLife.02069.
Kuokkanen, E., V. Šuštar, and P.K. Mattila. 2015. Molecular control of B cell activation and immunological synapse formation. *Traffic*. 16:311–326. doi:10.1111/tra.12257.
Kurosaki, T. 2002. Regulation of B-cell signal transduction by adaptor proteins. *Nature Reviews Immunology*. 2:354–363. doi:10.1038/nri801.
Li, J., W. Yin, Y. Jing, D. Kang, L. Yang, J. Cheng, Z. Yu, Z. Peng, X. Li, Y. Wen, X. Sun, B. Ren, and C. Liu. 2019. The coordination between B cell receptor signaling and the actin cytoskeleton during B cell activation. *Frontiers in Immunology*. 10:1–13. doi:10.3389/fimmu.2018.03096.
Lord, S.J., K.B. Velle, R.D. Mullins, and L.K. Fritz-Laylin. 2020. SuperPlots: Communicating reproducibility and variability in cell biology. *Journal of Cell Biology*. 219. doi:10.1083/jcb.202001064.
Martinez-Rivas, A., G.K. González-Quijano, S. Proa-Coronado, C. Séverac, and E. Dague. 2017. Methods of micropatterning and manipulation of cells for biomedical applications. *Micromachines*. 8. doi:10.3390/mi8120347.
Matsusaki, M., K. Sakaue, K. Kadowaki, and M. Akashi. 2013. Three-dimensional human tissue chips fabricated by rapid and automatic inkjet cell printing. *Advanced Healthcare Materials*. 2:534–539. doi:10.1002/adhm.201200299.
Mattila, P.K., F.D. Batista, and B. Treanor. 2016. Dynamics of the actin cytoskeleton mediates receptor cross talk: An emerging concept in tuning receptor signaling. *Journal of Cell Biology*. 212:267–280. doi:10.1083/jcb.201504137.
Metzger, H. 1978. The effect of antigen on antibodies: recent studies. *Contemporary topics in molecular immunology*. 7:119–152. doi:10.1007/978-1-4757-0779-3_4.
Müller, M.R., and A. Rao. 2010. NFAT, immunity and cancer: A transcription factor comes of age. *Nature Reviews Immunology*. 10:645–656. doi:10.1038/nri2818.
Okkenhaug, K., and J.A. Burger. 2015. PI3K signaling in normal B cells and chronic lymphocytic leukemia (CLL). *Current Topics in Microbiology and Immunology*. 393:123–142. doi:10.1007/82_2015_484.
Ozkan, M., T. Pisanic, J. Scheel, C. Barlow, S. Esener, and S.N. Bhatia. 2003. Electro-optical platform for the manipulation of live cells. *Langmuir*. 19:1532–1538. doi:10.1021/la0261848.
Pieper, K., B. Grimbacher, and H. Eibel. 2013. B-cell biology and development. *Journal of Allergy and Clinical Immunology*. 131:959–971. doi:10.1016/j.jaci.2013.01.046.
Rawlings, D.J., K. Sommer, and M.E. Moreno-García. 2006. The CARMA1 signalosome links the signalling machinery of adaptive and innate immunity in lymphocytes. *Nature Reviews Immunology*. 6:799–812. doi:10.1038/nri1944.
Schamel, W.W.A., and M. Reth. 2000. Monomeric and oligomeric complexes of the B cell antigen receptor. *Immunity*. 13:5–14. doi:10.1016/S1074-7613(00)00003-0.
Schiele, N.R., D.T. Corr, Y. Huang, N.A. Raof, Y. Xie, and D.B. Chrisey. 2010. Laser-based direct-write techniques for cell printing. *Biofabrication*. 2:32001. doi:10.1088/1758-5082/2/3/032001.
Shen, Z., S. Liu, X. Li, Z. Wan, Y. Mao, C. Chen, and W. Liu. 2019. Conformational change within the extracellular domain of B cell receptor in B cell activation upon antigen binding. *eLife*. 8:1–21. doi:10.7554/eLife.42271.

Strale, P.-O., A. Azioune, G. Bugnicourt, Y. Lecomte, M. Chahid, and V. Studer. 2016. Multiprotein Printing by Light-Induced Molecular Adsorption. *Advanced Materials*. 28:2024–2029. doi:https://doi.org/10.1002/adma.201504154.

Šuštar, V., M. Vainio, and P.K. Mattila. 2018. Visualization and quantitative analysis of the actin cytoskeleton upon B cell activation. *Methods in Molecular Biology*. 1707:243–257. doi:10.1007/978-1-4939-7474-0_18.

Théry, M. 2010. Micropatterning as a tool to decipher cell morphogenesis and functions. *Journal of Cell Science*. 123:4201–4213. doi:10.1242/jcs.075150.

Tolar, P., J. Hanna, P.D. Krueger, and S.K. Pierce. 2009a. The Constant Region of the Membrane Immunoglobulin Mediates B Cell-Receptor Clustering and Signaling in Response to Membrane Antigens. *Immunity*. 30:44–55. doi:https://doi.org/10.1016/j.immuni.2008.11.007.

Tolar, P., J. Hanna, P.D. Krueger, and S.K. Pierce. 2009b. The Constant Region of the Membrane Immunoglobulin Mediates B Cell-Receptor Clustering and Signaling in Response to Membrane Antigens. *Immunity*. 30:44–55. doi:10.1016/j.immuni.2008.11.007.

Tolar, P., H.W. Sohn, and S.K. Pierce. 2005. The initiation of antigen-induced B cell antigen receptor signaling viewed in living cells by fluorescence resonance energy transfer. *Nature Immunology*. 6:1168–1176. doi:10.1038/ni1262.

Walmsley, M.J., S.K.T. Ooi, L.F. Reynolds, S.H. Smith, S. Ruf, A. Mathiot, L. Vanes, D.A. Williams, M.P. Cancro, and V.L.J. Tybulewicz. 2003. Critical Roles for Rac1 and Rac2 GTPases in B Cell Development and Signaling. *Science*. 302:459. doi:10.1126/science.1089709.

Watson, J.L., S. Aich, B. Oller-Salvia, A.A. Drabek, S.C. Blacklow, J. Chin, and E. Derivery. 2021. High-efficacy subcellular micropatterning of proteins using fibrinogen anchors. *Journal of Cell Biology*. 220. doi:10.1083/jcb.202009063.

Wen, Y., Y. Jing, L. Yang, D. Kang, P. Jiang, N. Li, J. Cheng, J. Li, X. Li, Z. Peng, X. Sun, H. Miller, Z. Sui, Q. Gong, B. Ren, W. Yin, and C. Liu. 2019. The regulators of BCR signaling during B cell activation. *Blood Science*. 1.

Williams, G.T., C.J. Peaker, K.J. Patel, and M.S. Neuberger. 1994. The alpha/beta sheath and its cytoplasmic tyrosines are required for signaling by the B-cell antigen receptor but not for capping or for serine/threonine-kinase recruitment. *Proceedings of the National Academy of Sciences of the United States of America*. 91:474–478. doi:10.1073/pnas.91.2.474.

Woodruff, M.F.A., B. Reid, and K. James. 1967. Effect of Antilymphocytic Antibody and Antibody Fragments on Human Lymphocytes in vitro. *Nature*. 215:591–594. doi:10.1038/215591a0.

Yang, J., and M. Reth. 2010. Oligomeric organization of the B-cell antigen receptor on resting cells. *Nature*. 467:465–469. doi:10.1038/nature09357.

Yasuda, T. 2015. MAP kinase cascades in antigen receptor signaling and physiology. *Current Topics in Microbiology and Immunology*. 393:211–231. doi:10.1007/82_2015_481.

Zheng, Q., J. Lu, H. Chen, L. Huang, J. Cai, and Z. Xu. 2011. Application of inkjet printing technique for biological material delivery and antimicrobial assays. *Analytical Biochemistry*. 410:171–176. doi:10.1016/j.ab.2010.10.024.

9. Appendix

9.1 ImageJ macros

9.1.1 File conversion macro

```
//Closes results, event log and open images
function cleanUp() {
	requires("1.30e");
	if (isOpen("Results")) {
		selectWindow("Results");
		run("Close" );
	}
	if (isOpen("Log")) {
		selectWindow("Log");
		run("Close" );
	}
	while (nImages()>0) {
		selectImage(nImages());
		run("Close");
	}
}


// Gets image IDs of all open images and saves each image
dir = getDirectory("Choose a Directory");
ids=newArray(nImages); // creates an array of all open images
for (i=0;i<nImages;i++) {
	selectImage(i+1); // selects the next image in the array
	title = getTitle; // gets the title of the selected image
	print(title);
	saveAs("tiff", dir+title);
}

cleanUp();
```

9.1.2 Image cropping macro

```
//Closes results, log and open images
function cleanUp() {
	requires("1.30e");
	if (isOpen("Results")) {
		selectWindow("Results");
		run("Close" );
	}
	if (isOpen("Log")) {
		selectWindow("Log");
		run("Close" );
	}
	while (nImages()>0) {
		selectImage(nImages());
		run("Close");
	}
}


//Requests the user for a directory where the input images are
inputf=getDirectory(getString("Give path of image folder",
"default"));

//Request the user for a directory where the output TIFF will be saved
```

```
outputf=getDirectory(getString("Give path of results folder",
"default"));

filelist = getFileList(inputf) // Creates a list of files in the input
directory

// Requests the user for a string of text which is later used as a
template for file name generation
NameForOutputImage=getString("Name for result file",
"20200000_min_DAPI_pPLCg2-488_fibrinogen-546_ph-670");

number=0; // Variable representing the number of cells in the input
image. Is set as 0 initially

// This loop iterates through all the files in the input directory
once
for (i = 0; i < lengthOf(filelist); i++) {

	// If the item (image file) in the list at place i ends with
	".tif" the following commands are executed
	if (endsWith(filelist[i], ".tif")) {
		open(inputf + File.separator + filelist[i]); // Open
		image in the list at place i
		Stack.setChannel(4); // Display channel 4

		// Requests the user for how many cells are in the image
		Ncells = getNumber("How many cells do you want to
		analyse?", 1);

		// The loop iterates the number of times corresponding
		to the number of cells in the image
		for (j = 0; j < Ncells; j++) {

			// Creates a rectangle selection box
			makeRectangle(0, 0, 200, 200);

			// Waits for the user to allign the box with the
			cell
			waitForUser("Move to crop the cell");

			// Creates a cropped image at the site of the
			rectangle selection

			run("Duplicate...", "title=duplicate duplicate");

			selectWindow("duplicate"); // Selects the cropped
			image

			// Saves the cropped image at the output
			directory with the name specified by the user
			saveAs("tiff", outputf+NameForOutputImage+"-
			"+number);
			waitForUser;

			// Closes the image
			selectWindow(NameForOutputImage+"-
			"+number+".tif");
			close();

			number++; // Iterates the cell number by 1

		}
		cleanUp();
	}
```

```
}
```

9.1.3 Image measurement macro

```
// Closes the "Results" and "Log" windows and all image windows
function cleanUp() {
	requires("1.30e");
	if (isOpen("Results")) {
		selectWindow("Results");
		run("Close" );
	}
	if (isOpen("Log")) {
		selectWindow("Log");
		run("Close" );
	}
	while (nImages()>0) {
		selectImage(nImages());
		run("Close");
	}
}

//Requests the user for a directory where the input images are
imagefolder=getDirectory(getString("Give path of image folder",
"default"));

//Request the user for a directory where the output .CSV files will be
stored
resultsfolder=getDirectory(getString("Give path of results folder",
"default"));

print(imagefolder);

//Generates a list of the input files in the input directory
filelist = getFileList(imagefolder)

//Asks the user for the channel where the micropatterns are visible
patt=getString("Which channel are the patterns?", "3");

//Asks the user for the channel which is used to threshold the cell
signal=getString("Which channel do you want to use to mask the
cells?", "4");

//Asks the user for a filename for the results files
NameForResults=getString("Name for result file", "0min-Hu2_a_thres-
dill_ero-A_part");

//setBatchMode(true); //batch mode on

//Loop that goes opens all the files in succession and does analysis
on each of them separately
for (i = 0; i < lengthOf(filelist); i++) {
	if (endsWith(filelist[i], ".tif")) {
		open(imagefolder + File.separator + filelist[i]);

		//Gets the title of the opened image
		title=getTitle();
		print(title);

		extension=lengthOf(title)-4;
		print(extension);
		plainName=substring(title,0,extension);
		print(plainName);
		run("Duplicate...", "title=mask duplicate");
```

```
//Masking patterns
selectWindow("mask");
run("Split Channels");
selectWindow("C"+patt+"-mask");



run("Auto Threshold", "method=Huang2 white");
selectWindow("C"+patt+"-mask");
run("Make Binary");
selectWindow("C"+patt+"-mask");
run("Fill Holes");


//Masking cells
selectWindow("C"+signal+"-mask");
run("Auto Threshold", "method=Huang2 white");

//Filling holes of cell masks
selectWindow("C"+signal+"-mask");
run("Make Binary");
selectWindow("C"+signal+"-mask");
setOption("BlackBackground", true);

//Dilate the binary image
for (k = 0; k < 5; k++) {
        run("Dilate");
}
k=0;
//waitForUser;


run("Fill Holes");

run("Options...", "iterations=1 count=1 black pad");

//Erode the binary image
for (y = 0; y < 5; y++) {
        run("Erode");
}
y=0;

//Adding ROIs
selectWindow("C"+signal+"-mask");
run("Analyze Particles...", "size=20-Infinity
show=Overlay
display include add");
selectWindow("C"+patt+"-mask");
run("Analyze Particles...", "size=20-Infinity
show=Overlay
display include exclude add");


//waitForUser("Edit ROIs");


//Subtracting ROIs from another
roiManager("select", 0);
setKeyDown("alt");
roiManager("select", 1);
setKeyDown("none");
roiManager("add");
roiManager("select", 2);
```

```
                roiManager("rename", "Doughnut");

                //waitForUser;

                //Measuring final ROIS
                for (q = 1; q < 5; q++) {
                        roiManager("deselect");
                        selectWindow(title);
                        Stack.setChannel(q);
                        roiManager("multi-measure");
                        saveAs("results", resultsfolder+NameForResults+"-
                        "+i+"Ch"+q+".csv");
                        print("Saving results done");
                        //waitForUser;

                }
                //waitForUser;
                roiManager("Delete");
                cleanUp();
                }
        }

//setBatchMode(false); //exit batch mode

cleanUp();
```